ELSEVIER

Coordination Chemistry Reviews
178–180 (1998) 1647–1677

COORDINATION CHEMISTRY REVIEWS

Organometallic chemistry of group VI metals in the void space of zeolites

Claude Brémard *

Laboratoire de Spectrochimie Infrarouge et Raman, UPR-CNRS 2631, Centre d'Etudes et de Recherches Lasers et Applications, Bâtiment C5, Université des Sciences et Technologies de Lille I, 59655 Villeneuve d'Ascq, Cédex, France

Received 6 January 1998; accepted 26 February 1998

Contents

Abstract 1648
1. Introduction 1648
2. The zeolites 1649
3. Experimental techniques 1651
4. Theoretical methods 1653
5. Organization and dynamics of $M(CO)_6$ (M = Cr, Mo, W) in the void space of M'_nFAU (n = 0, 56, 85; M' = Li^+, Na^+, K^+, Rb^+, Cs^+, H^+) 1654
6. $M(CO)_p$ (p = 5–3) Subcarbonyl species and naked metallic clusters in the void space of M'_nFAU (n = 0, 56, 85; M' = Li^+, Na^+, K^+, Rb^+, Cs^+ 1658
7. Organization and dynamics of organic ligand (C_6H_6, C_5H_5N, $P(CH_3)_3$) in the void space of M'_nFAU (N = 0, 56, 85; M' = Na^+, K^+, Cs^+, H^+) 1661
7.1. C_6H_6 1661
7.2. C_5H_5N 1662
7.3. $P(CH_3)_3$ 1663
8. Organization, dynamics of cooperative effects of $M(CO)_6$ and C_6H_6 or C_5H_5N, or $P(CH_3)_3$) cosorbed in Na_nFAU (n = 0, 56, 85) 1663
8.1. $M(CO)_6$–C_6H_6 1663
8.2. $M(CO)_6$–C_5H_5N 1666
8.3. $M(CO)_6$–$P(CH_3)_3N$ 1667
9. Investigations of the intrazeolite reactions between $M(CO)_6$ and ligands (C_6H_6, C_5H_5N, $P(CH_3)_3$) in Na_nFAU (n = 0, 56, 85). Identification of the reaction products within the zeolitic porous space 1667
9.1. $M(CO)_6$–C_6H_6 1667
9.2. $M(CO)_6$–C_5H_5N 1669
9.3. $M(CO)_6$–$P(CH_3)_3$ 1669
10. Energetics and sorption sites of the reaction products in the zeolitic porous space 1670
11. Reaction pathways between $M(CO)_6$ (M = Cr, Mo, W) and ligands within the void space of faujasitic zeolites. Conclusions 1673

* Fax: +33 20 436755; e-mail: claude.bremard@univ-lille1.fr

0010-8545/98/$ – see front matter
PII S0010-8545(98)00074-5

Acknowledgements 1675
References 1675

Abstract

Many salient features about the structures, dynamics and transport of organometallic complexes of group VI metals ($M(CO)_6$, M=Cr, Mo, W) and ligands (C_6H_6, C_5H_5N, $P(CH_3)_3$) occluded within the void space of faujasitic zeolites have been deduced from X-ray and neutron diffraction, EXAFS, inelastic neutron scattering, RMN, IR absorption, Raman scattering investigations as well as from theoretical methods. The faujasitic zeolites are porous crystalline aluminosilicates with $M'_n[(SiO_2)_{192-n}(AlO_2)_n]$ (M'_nFAU) formulae per unit cell, the $M(CO)_6$ and ligand molecules can gain free access to the inner void space (supercages) through the smallest section called the windows. The silicon–aluminum ratios (Si/Al) of the framework are found to be in the 1–100 range whereas M'^+ cations compensate the AlO_2^- charges of the framework ($M'^+ = H^+$, Li^+, Na^+, K^+, Rb^+, Cs^+). From the *in situ* spectroscopic investigations and molecular modeling a coherent picture of the reactions between $M(CO)_6$ and ligands under thermal activation has been drawn as a function of the aluminum content of the zeolite. Among the available *in situ* spectroscopic investigations (far-IR, Raman, UV–visible, NMR) diffuse reflectance infrared Fourier transform spectroscopy (DRIFTS) in the mid-IR region provides an efficient tool for dehydration, sorption and cosorption as well as subsequent reactions under thermal activation even at low coverage. In siliceous faujasite (Si/Al=100) the $M(CO)_6$ and ligand molecules are randomly distributed within the void space and the molecular motions approach the rapid isotropic limits of liquids. The chemical behavior upon thermal activation is found to be analogous to that observed in solution. In Na_{56}FAU (Si/Al=2.5) the reagents are trapped in well-defined sorption sites in close proximity. Upon gentle thermal activation a fast reaction occurs to form $M(CO)_3(\eta^6\text{-}C_6H_6)$ or $Mo(CO)_3(C_5H_5N)_3$, or $Mo(CO)_4(P(CH_3)_3)_2$ as major species inside the supercage through a concerted mechanism including the electrostatic field and the basicity of the framework oxygens. In Na_{85}FAU (Si/Al=1.25) the $M(CO)_6$ and ligand molecules are not encapsulated in close proximity. $M(CO)_6$ reacts thermally in the void space in the absence of ligand to lose sequentially three CO ligands and form predominantly anchored $M(CO)_3(O_z)_3$ species in which the three vacant coordination sites are occupied by three O_z framework oxygens. The substitution kinetics have been interpreted on the basis of structure and dynamics of reactant and product guests in the zeolites. The kinetics data reveal that the available porous volume of zeolite can provide a precisely defined activating environment to obtain faster reactions than in homogeneous media. The dynamics of the supramolecular assembly of $M(CO)_6$, ligands and extraframework cations M'^+ in the vicinity of the oxygen atoms of the inner surface can undergo rapid and specific organometallic reactions under geometry, size, shape and electrostatic constraints.

Keywords: Zeolites; Carbonyl metals; Diffuse reflectance; IR spectroscopy

1. Introduction

Organometallic chemistry supported on inorganic matrices has been extensively studied and published [1–4]. Particularly, much research devoted to the organometal-

lic chemistry within the channel network of zeolites has been reported previously [5–37]. Zeolites which are crystalline aluminosilicates offer an advantage over many of the other supports, such as alumina or silica in that the regular arrangement of pores and channels helps to establish the organized location in the void space for the guest molecules.

The first role of the porous material is to reduce the mobility or to immobilize the organometallic species within the void space.

The second role of the zeolite is the molecular sieves and nanoreactor functions. Thus, only molecules of a certain size and shape will be able to gain access to the nanoreactors.

The third role of the porous networks is to impart selectivity of the reaction through the orientation of the molecules inside the nanoreactors.

The hexacarbonyl group VI metals $M(CO)_6$ (M = Cr, Mo, W) occluded in zeolites were found to be precursors of efficient catalytic systems for Fisher–Tropsch, metathesis of olefins, hydrogenation, isomerization or hydrodesulfuration processes [2,34–36]. In addition, $M(CO)_6$ occluded in zeolites can provide highly organized nanoassemblies of molybdenum or tungsten oxides encapsulated within the network of zeolites [37]. To pursue the ultimate goal of creating "material by design", a fundamental knowledge of molecular interactions and reaction mechanisms inside the void space is in demand. Several questions such as the location, the dynamics and the reactions between $M(CO)_6$ and several ligands and reactifs in zeolites have been raised.

In this account, the more recent and significant research efforts involving the chemistry of group VI metal hexacarbonyls with ligands such as arenes and phosphines in zeolite void space and their relation with catalytic processes are described and summarized. The emphasis of the paper is mainly set on the *in situ* diffuse reflectance infrared Fourier transform spectroscopic (DRIFTS) investigations and on the molecular modeling of the sorbate location and transport properties within the void space.

2. The zeolites

Among the porous materials a lot of crystalline porous materials are available including large pore aluminosilicates (zeolites), aluminophosphates, metalloaluminosilicates etc... [38,39]. However the main published work concerning the sorption of $M(CO)_6$ involve large pore zeolites with 12-membered rings, namely the cubic X and Y faujasitic zeolites abbreviated hereafter as FAU zeolites. Nevertheless, some aspects of the sorption of $M(CO)_6$ in type L zeolite and in the hexagonal EMT variant of the faujasite have been reported [17,40]. However the intrazeolite organometallic chemistry was found to be well characterized for the FAU zeolites which are available in a large domain of Si/Al framework composition and of extraframework cations.

A series of books have been devoted to the syntheses and structures of zeolites [38,39]. For the purpose of this review, the FAU structures are briefly described.

The faujasitic FAU zeolites are crystalline aluminosilicates with $M'_n[(SiO_2)_{192-n}(AlO_2)_n].zH_2O$ formulae per unit cell. The silicon–aluminum ratios (Si/Al) of the framework are found to be in the 1–100 range, whereas the extraframework M'^+ cations compensate the AlO_2^- charges of the framework. The Na^+ cation of the as-synthesized zeolites can be exhaustively exchanged for specific purpose by other cations (alkali metals ($M'=Li^+$, K^+, Rb^+, Cs^+), alkaline earth metals or proton H^+) without altering the framework structure. The exhaustive evacuation of the water molecules of the as-synthesized zeolites is necessary to obtain the effective porous materials. The dehydration occurs with the retention of the framework structure and some modification of the extraframework cation sites and occupancy.

$$M'_n[(SiO_2)_{192-n}(AlO_2)_n].zH_2O \rightarrow M'_n[(SiO_2)_{192-n}(AlO_2)_n] + zH_2O \quad (1)$$

The network of 4- and 6-membered rings built with SiO_4 or AlO_4 tetrahedra through oxo bridges form cubooctrahedra or sodalite building blocks. These units are linked together through double 6-rings. The resulting spatial arrangement delimits spherical cavities called supercages. The 1.3 nm diameter supercage is accessed through four 0.75 nm free diameter circular apertures. Fig. 1

The M′ extraframework cations are found to be located at sites I, I′, II and III with partial occupancies according to the zeolite. Site I is located within the hexagonal prism site, site I′ occupies the 6-ring center within the sodalite cages, while sites II and II are located in the vicinity of the centers of the 6- and 4-rings, respectively, within the supercages. Recent X-ray and neutron diffraction determinations of bare zeolites are available for purely siliceous FAU [41], and aluminated Na_nFAU ($n=56$, 88) [42–44], $Li_{56}FAU$ [45], $K_{56}FAU$ [46], $Cs_{56}FAU$ [47] and $H_{56}FAU$ zeolites

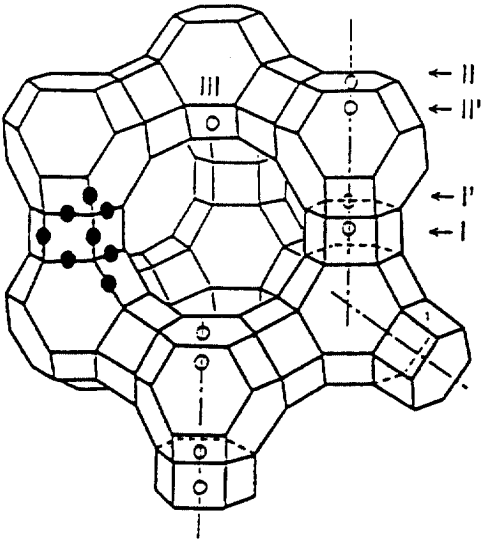

Fig. 1. Conventional view of FAU zeolite centered at the supercage. Oxygen atoms O(1)–(4) and cation sites (I, I′, II, II′, III) are shown.

[48]. They provide the average atomic positions of all the atoms and the partial occupancy of the cation sites. However, the Si, Al order was not obtained by the diffraction studies, a model of random Al siting obeying the Loewenstein rule (absence of Al–O–Al linkages) is in accurate agreement with the ^{29}Si NMR data [49].

The $M(CO)_6$ molecules with globular structures (static diameter in the 0.74–0.76 nm range including the van der Waals radii), the trimethylphosphine and the aromatics with flat-shape gain free access to the inner void space (supercages) through the smallest sections called the windows. With respect to further investigations of the faujasitic zeolite/sorbate system, the flexibility of the inner void space is especially interesting. The windows have to be passed by diffusing particles and therefore can be considered as a transition-state region for diffusion processes [50–52]. Even small deformations of the window size may lead to drastic changes in the energies of activation if the dimensions of the sorbates are comparable to the size of the windows. Two aspects of the window flexibility, the diameter and the area, are examined. The diameter is though to be important to flat-shaped molecules like arenes, the area of the window may become a more relevant criterion for guests with globular structures. In addition, the diffusion processes depend on the dynamics of the extraframework cations and particularly on the cations located in the available void space (sites II and III) of the porous materials [53]. The vibrational and NMR spectroscopies in combination with molecular dynamics calculations provide valuable information in this field.

Because of much greater radius of the framework O atoms relative to the Si^{4+} and Al^{3+} centers, the curved inside of the supercages is dominated by the oxide sheath in which the Si^{4+} and Al^{3+} sites are effectively "buried" from view. The extraframework cations interact mainly coulombically with three and four nearest-neighbor O atoms of the 6- and 4-rings, respectively. The extraframework cations in sites II and III are "half naked" and considered as coordinately unsaturated. Gigantic electrostatic fields, estimated to be of the order of 10^6–10^8 V cm^{-1} are associated with these cationic "open coordination" sites [31]. These can have massive polarizing effects on encapsulated guests and play a key role in the coordination chemistry of the so-called zeolate ligand. By thoughtful changes of the Si/Al ratio of the framework and choice of extraframework cations, one has the possibility to change the electron density of the O atoms (Lewis base centers) and to reduce the available void space. The main published work concerning the intrazeolite carbonyl metal chemistry is devoted to faujasitic zeolite samples, $M'_n[(SiO_2)_{192-n}(AlO_2)_n]$, with Si/Al in the range 1.27–100, the extraframework cations are $M'^+ = H^+$, Li^+, Na^+, K^+, Rb^+ and Cs^+. The dehydrated faujasitic zeolites are available as powdered samples. The average crystallite size of all the zeolite samples is approximately 0.5 μm, the average particle size is 3 μm.

3. Experimental techniques

The water molecules were removed from the porous network of the crude zeolites by calcination. Owing to the sensibility to moisture and oxygen of both bare zeolites

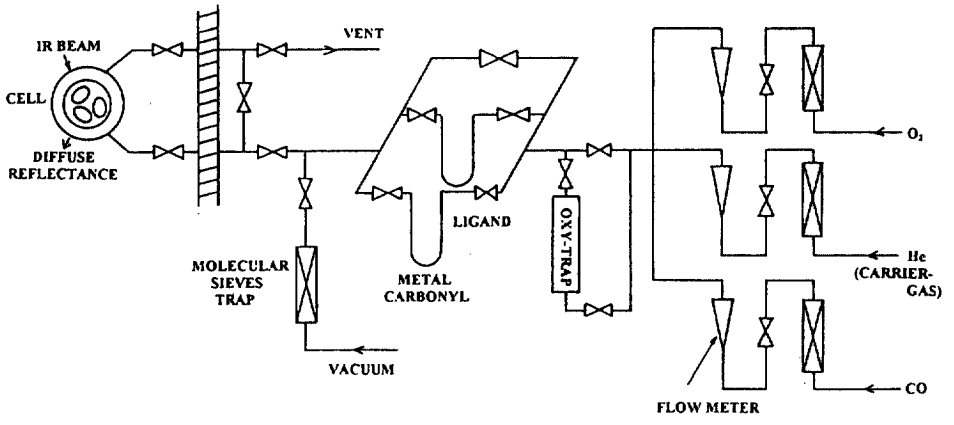

Fig. 2. Experimental setup for *in situ* DRIFTS investigations of the dehydration, carbonyl metal and ligand loadings and thermal treatment of zeolites. The key part of the DRIFTS apparatus is a heatable evacuable cell operating from 100 to 800 K.

and organometallic species all the sorptions, cosorptions, reactions and samplings are done under an inert atmosphere.

Many structural as well as dynamic details of the precursors $M(CO)_6$, C_6R_6, PR_3 etc... and reaction products within the void space of the zeolites have been elucidated through the use of such techniques as electron microscopy (HR-TEM) [54]; powdered X-ray (XRD) and neutron diffraction (ND) [42]; X-ray absorption (EXAFS) [19,23]; ^{13}C, ^{23}Na, ^{31}P, ^{95}Mo, ^{129}Xe NMR [24,31,36,55,56]; IR absorption [16–31]; and Raman scattering [26,27,57,58].

The techniques of quantitative PXRD, STEM-EDX, XPS, FTIR, gas chromatography, elementary analysis and gravimetry have been applied to examine the porous material from the precursor stage through each of the sorption, cosorption and reaction sequences at low and high loading [31]. Particularly, the diffuse reflectance FTIR spectroscopy (DRIFTS) provides an efficient tool for *in situ* investigation of the dehydration, sorption and cosorption as well as subsequent reactions under thermal activation even at low coverage.

The DRIFTS technique allows the use of crude powders as zeolite samples. The details of the experimental setup were reported previously [26,27,59]. Fig. 2

The sequence of steps in a typical experiment was as follow: the powdered zeolite sample is introduced into an evacuable heatable cell connected to vacuum and gas lines. The sample is pumped down to low pressure and heated stepwise to 700 K, and then O_2 gas is admitted into the cell. After 6 h, the sample is pumped down to low pressure and then cooled to room temperature. Dry He carrier gas is drawn through the dehydrated zeolite. Side arms containing $M(CO)_6$ and/or volatile ligands are opened for different periods. Spectra can be recorded during and after the equilibrium phase at different temperatures. The hydration level and the loading of $M(CO)_6$ and ligands are monitored through the IR intensity using the Kubelka–Munk scale, $F(R)=(1-R)^2/2R=K/S$. R represents the ratio of the diffuse

reflectance of the loaded zeolite to that of the dehydrated neat zeolite, K designates an absorption coefficient proportional to the concentration of the absorbing species and S is the scattering coefficient of the powder [60].

4. Theoretical methods

The predictions of siting locations, conformation, dynamics and energetics of sorbates were found to provide pertinent information in this field through Monte Carlo (MC) simulations and molecular dynamics (MD) calculations. The structure predictions are particularly useful for sorption and cosorption at low coverage, where diffraction results are not available.

These theoretical methods are based on classical mechanics. The zeolite (Z) atoms and the sorbate (S) atoms are assumed to interact through interatomic potential for intramolecular (bond stretching, angle bending and torsional angle) and intermolecular (van der Waals) interactions. The electrostatic interactions are modeled with a point-charge potential. The charge distribution within the M_n^iFAU structures is derived from previous work [61]. The structural parameters and charge estimates of sorbates are obtained from structural determination and/or quantum chemical population analysis [62–70]. The polarizability interactions between the sorbate and zeolite atoms are not taken into account explicitly. This is expected to contribute no more than 10% to the electrostatic interactions. The basis and the details of the calculations were given in several papers reported previously [26,27].

The MC simulations of the sorption and cosorption at fixed pressures were carried out using the grand canonical ensemble (GCMC); in this the number of particles in the system is determined by the fixed chemical potential of each species. One Monte Carlo step consists of four parts (create, destroy, translate and rotate a molecule). The resulting analysis can be compared to the experimental saturation loadings and the sorption energetics.

In MD simulations we follow the evolution of an ensemble of particles over a time period. This ensemble, often called the MD box, represents the sample. The integration of the laws of classical mechanics permits the determination of the positions and velocities of all atoms as a function of time. A statistical study of these trajectories yields useful information about the system and the results can be compared to experimental structural data and diffusion coefficients. The vibrational density of states, IR and Raman spectra can be simulated through the Fourier transform of the velocity, dipole and polarizability autocorrelation functions, respectively [58].

It should be noted that the structures and vibrational spectra of bare M_n^iFAU zeolites are reasonably reproduced by the calculations, whereas the predicted location siting, vibrational spectra and sorption energy of C_6H_6 occluded in FAU and $Na_{56}FAU$ are in accurate agreement with the experimental results [41,71,72]. All these things suggest that the concept of interatomic force field and localized partial charge can be used efficiently to reproduce some key experimental results with a correct approximation. Unfortunately, the organometallic reactivity within the void space can be explained only through quantic molecular dynamic concepts and till now to our knowledge no significant result in this field has been reported.

5. Organization and dynamics of $M(CO)_6$ (M = Cr, Mo, W) in the void space of M'_n FAU (n = 0, 56, 85; M′ = Li^+, Na^+, K^+, Rb^+, Cs^+, H^+)

Surprisingly, to our knowledge no crystallographic determination of the location of the hexacarbonyl metals in M'_nFAU using Rietweld methods was reported previously. However, a neutron diffraction study of $Mo(CO)_6$ occluded in K_{56}FAU is in progress in our laboratory, but the expected result will be representative of $Mo(CO)_6$ occluded at high coverage. The saturation loading of $M(CO)_6$ (M = Cr, Mo, W) from the vapor phase into fully dehydrated M'_{56}FAU (M′ = H^+, Li^+, Na^+, K^+, Rb^+, Cs^+) amounts to 16 $M(CO)_6$/unit cell. EXAFS structure analysis of 8 $M(CO)_6$–M'_{56}FAU (M = Mo, W; M′ = Na^+, Rb^+) using the Mo K-edge, W LIII-edge and Rb K-edge, demonstrates that the integrity of the $M(CO)_6$ guest is maintained intact on encapsulation at room temperature in M'_nFAU with Si/Al > 2 or n < 80 [19,26]. The characteristic bond length estimates of occluded $Mo(CO)_6$ in Rb_{56}FAU are in reasonable agreement with the expected values deduced from Monte Carlo simulations [19]. Structural information can be deduced from the GCMC simulations: at saturation loading, each $M(CO)_6$ is located in the vicinity of each 12-ring window of M'_{56}FAU (M′ = Li^+, Na^+, K^+, Rb^+, Cs^+). In the case of bulky cations (K^+, Rb^+, Cs^+), the predicted structural parameters found at low filling remain unaffected at saturation loading [26]. In the case of smaller cations (Li^+, Na^+), the predicted structural parameters found at high filling differ slightly from those predicted at low coverage and the nearest Mo–Mo distance is found to be short. In other words, the $M(CO)_6$ molecules associate in pairs in M'_{56}FAU (M′ = Li^+, Na^+) whereas with M′ = K^+, Rb^+, Cs^+ the occluded $M(CO)_6$ can be considered as isolated molecules. The IR absorption and Raman scattering results of the 16 $M(CO)_6$–M'_{56}FAU samples were found to be in accurate agreement with the conclusions deduced from GCMC simulations [26]. The prediction of the $M(CO)_6$ sorption at saturation in the M'_{85}FAU zeolites with high aluminum content remains purely speculative because of the intrazeolite decomposition of $M(CO)_6$. Fig. 3

The ^{23}Na MAS and double rotation (DOR) NMR spectra of the 16 $Mo(CO)_6$–Na_{56}FAU sample show three components distinguished by the corresponding quadrupole coupling constants (QCC). The component corresponding to the Na^+ cations located within the supercage (site II) provides evidence of the interactions between the Na^+ in site II and $Mo(CO)_6$ [36]. On the basis of ^{95}Mo T_1 measurements, it is confirmed that $Mo(CO)_6$ experiences significant rotational freedom in the void space of faujasitic zeolites [55]. The ambient temperature rotational correlation time is found to be 4×10^{-9} s, a value three orders of magnitude longer than that reported for $Mo(CO)_6$ in solution and probably longer than that expected in siliceous FAU. The jump rate of $Mo(CO)_6$ to neighboring sites must be slow and the local anisotropic reorientation fast on the ^{13}C NMR time scale.

The dynamics of the framework and extraframework cations were taken into account explicitly in the MD study of the mobility of $Mo(CO)_6$ in the void space of Na_{56}FAU. The jump rate of $Mo(CO)_6$ was found to be slow compared to the vibrational motion time scales of the $Mo(CO)_6$ molecule and Na^+ cations. The

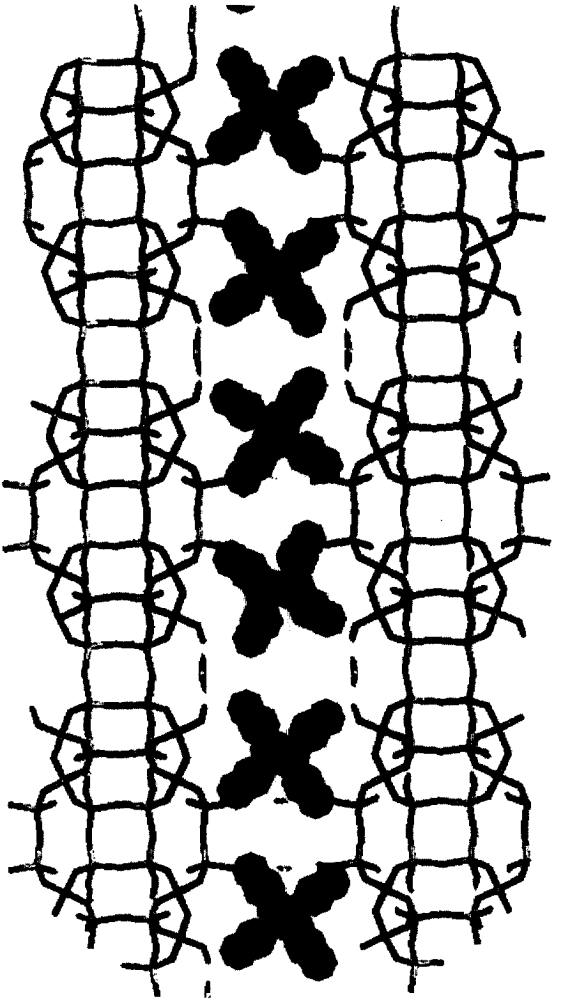

Fig. 3. Z-clipping (thickness 1 nm) in the (010) plane showing the zeolite framework (O, Si, Al cylinders) and the predicted location of $Mo(CO)_6$ molecules along the channel at saturation filling in $K_{56}FAU$ (16 $Mo(CO)_6$ per unit cell). The extraframework K^+ cations are omitted for clarity.

calculated vibrational density of states was found to be slightly modified by the proximity of $Mo(CO)_6$ in the void space. This conclusion is in accurate agreement with the previously reported far-IR absorption spectra of 16 $Mo(CO)_6$–$Na_{56}FAU$. However, as previously reported for bare M'_nFAU zeolites, no specific assignment of a far-IR band corresponding to a Na^+ vibrational motion in individual sites (I, I′, II) can be made [73,74].

In order to avoid the problem of pore blocking which can hinder the intracrystalline diffusion at high coverage, the experiments at low coverage are more representative of the effective reaction conditions.

The DRIFTS technique allows the use of powders as samples, so the molecules can diffuse easily in the intercrystalline space. The DRIFTS technique is particularly sensitive to the presence of carbonyl species and provides valuable information through the ν(CO) stretching modes even at very low loading. The free octahedral $M(CO)_6$ molecule has three fundamental vibrations in the ν(CO) region: nondegenerate $\nu_1(A_{1g})$ near 2120 cm^{-1} (Raman-active), doubly degenerate $\nu_3(E_g)$ near 2020 cm^{-1} (Raman-active) and triply degenerate $\nu_6(F_{1u})$ near 2000 cm^{-1} (IR-active). When the DRIFTS spectra were recorded immediately after the sorption of $M(CO)_6$ from the vapor phase into calcined M'_nFAU all the spectra displayed a structureless broad band centered near 1980 cm^{-1}, and no splitting was observed upon cooling to 100 K. The ν(CO) patterns have a better resemblance to the ν(CO) spectra of the corresponding $M(CO)_6$ in solution, whereas no direct analogy was found with the bulk state of solid $M(CO)_6$. Upon standing, the original spectra progressively develop into more complex features typical of the zeolite host. This can be explained in terms of a diffusion control of $M(CO)_6$ in the voids of the microcrystals to an order of the guests. The migration rate of $M(CO)_6$ within the pore system to a definite sorption site is actually slow and can be increased under gentle warming [19,20,26].

For the purely siliceous FAU zeolite, at very low coverage, when the system was allowed to reach equilibrium over 48 h, only one ν(CO) absorption ($\sim$1980 cm^{-1}) was observed, whereas several well-defined ν(CO) absorptions were detected for M'_{56}FAU, arising from the lifting of the different degeneracies. Significant narrowing of the bands was obtained upon cooling to 100 K [26].

It is well established that sorption of $M(CO)_6$ into the M'_nFAU zeolites (Si/Al > 2) at ambient temperature results in retention of the structural integrity of the $M(CO)_6$ species over several months at room temperature. The IR spectroscopic behaviors were found to be analogous for M = Cr, Mo, W with small frequency shifts.

$$p\mathrm{M(CO)_6} + \mathrm{FAU} \rightarrow p\mathrm{M(CO)_6\text{–}FAU} \quad (p = 0\text{–}16) \tag{2}$$

$$p\mathrm{M(CO)_6} + \mathrm{M'_{56}FAU} \rightarrow p\mathrm{M(CO)_6\text{–}M'_{56}FAU} \quad (p = 0\text{–}16) \tag{3}$$

$$p\mathrm{M(CO)_6} + \mathrm{M'_{85}FAU} \rightarrow p\text{subcarbonyl–M'}_{85}\mathrm{FAU} + \mathrm{CO}\nearrow \tag{4}$$

At very low coverage, typically 1 $M(CO)_6$ per 20 unit cells of siliceous FAU, the sorption undergoes isotropic perturbation of the O_h symmetry which results in weak band broadening of the $\nu_6(F_{1u})$ IR-active mode. The similarity between the IR absorption spectra in solution and occluded in FAU provides clear evidence that the motion of the $M(CO)_6$ molecule within the void space approaches the rapid isotropic limit characteristic of a liquid at room temperature [26].

In contrast, in zeolites M'_{56}FAU with small cations ($M' = Li^+$, Na^+), the DRIFTS spectra of the $M(CO)_6$ guests exhibit six well-defined ν(CO) absorption patterns which are characteristic of a well-defined sorption site with low local symmetry. The low local symmetry promotes the breakdown of the selection rules of the free molecules and induces the splitting of the $\nu_6(F_{1u})$ band into three components and the appearance of the $\nu_1(A_{1g})$ and the appearance and splitting of the $\nu_3(E_g)$ IR-forbidden modes of the free molecule.

In the case of M'_nFAU zeolites with bulky cations ($M' = K^+$, Rb^+, Cs^+) the local symmetry of the guest was found to be C_{3v} with respect to the four observed ν(CO) IR bands. The two prominent bands arise from the splitting of the IR-active $\nu_6(F_{1u})$ mode into A_1 and E modes and the two weaker bands A_1 and E arise from the IR-forbidden $\nu_1(A_{1g})$ and $\nu_3(E_g)$ modes of the free molecule, respectively.

These experimental spectroscopic results are supported by MC and MD calculations of the sorption at fixed loading, typically 1 $M(CO)_6$ per unit cell. The expected energy of sorption of $M(CO)_6$ is found to increase with the aluminum content of the host and reflect the dominating influence of the cation–sorbate interactions. The positions occupied by $M(CO)_6$ in the completely siliceous FAU are mainly distributed between the four windows of the supercages. The absence of a well-defined sorption site indicates that the net potential surface accessible to the molecule is fairly uniform in the void space of FAU. The simulated IR absorption spectra of occluded $M(CO)_6$ are deduced by the Fourier transform of the autocorrelation function of the dipole obtained from the MD calculations [75]. They are in accurate agreement with the experimental DRIFT spectra. $M(CO)_6$ is undergoing rapid rotational and translational motions upon the vibrational spectroscopy time scale even at low temperature.

Fig. 4 depicts the most probable location of $Mo(CO)_6$ in the Na_{56}FAU void space. More than 95% of the center of mass sampled during the simulations is located within an isosurface of the probability density of Mo. This isosurface is approxi-

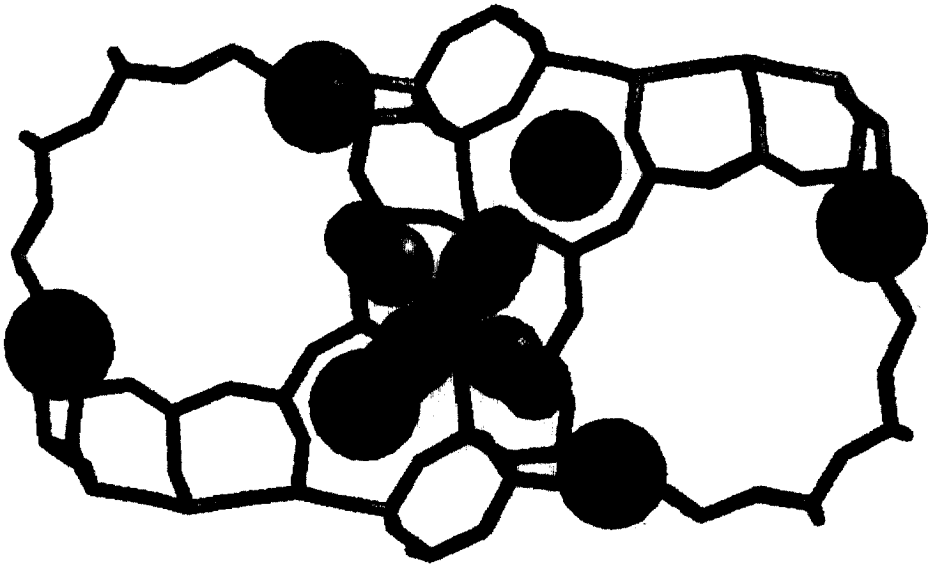

Fig. 4. Predicted sorption site of $Mo(CO)_6$ in Na_{56}FAU at low coverage (1 $Mo(CO)_6$ per unit cell). Two supercages of zeolite Na_{56}FAU and the interconnecting 12-ring window of diameter 0.8 nm. The cylinders represent the O, Si, Al atoms of the zeolite framework. The large shaded spheres represent the Na^+ cation, the medium black and shaded spheres represent O and C atoms of $Mo(CO)_6$, respectively.

mately a 1.3-Å diameter sphere situated in the vicinity of the center of the window of the supercage with a maximum number of surrounding cations. The local symmetry was found to be close to C_{2v} for small cations ($M' = Li^+$, Na^+) and is in accurate agreement with the DRIFTS investigations [26]. The locations of the sorbates were found analogous for all the $M(CO)_6$ molecules (M = Cr, Mo, W). The substitution in Na_{56}FAU of the Na^+ cations by bulky cations such as K^+, Rb^+, Cs^+ dramatically modifies the sorption properties. As the size of M′ increases, $M(CO)_6$ is constrained to reside in the center of the window with a C_{3v} local symmetry as deduced from the IR absorption results [19,26].

Following such a vapor phase transfer procedure, with prolonged gentle annealing one finds that the one band ν(CO) pattern remains essentially invariant to the $M(CO)_6$ coverage in purely siliceous FAU. The weak broadening of the ν(CO) band as a function of the filling is in agreement with interactions between molecules undergoing rapid motions within the voids. This finding is consistent with the inability to locate any sorbate in FAU by MC simulations.

In M'_{56}FAU with bulky cations ($M' = K^+$, Rb^+, Cs^+), the vibrational spectra are essentially invariant to the $M(CO)_6$ coverage. The vibrational spectroscopic behavior reveals that $M(CO)_6$ are rigidly held within the windows of the supercages and vibrate independently from each other. The GCMC simulations at fixed pressure indicate that the sorption sites are randomly filled as much as at saturation without any significant sorbate–sorbate interactions.

In contrast, for aluminated zeolites M_{56}FAU with small cations ($M' = Li^+$, Na^+) the DRIFTS ν(CO) patterns change markedly as the average loading is increased from 4 $Mo(CO)_6$/unit cell to saturation (16 $Mo(CO)_6$/unit cell). From DRIFTS results and GCMC simulations, it is suggested that the $Mo(CO)_6$ molecules are predominantly entrapped as isolated molecules in Na_{56}FAU at average loading lower than 4 $Mo(CO)_6$/unit cell, whereas at higher loading the intracavity distribution is primarily pairwise with unoccupied supercages. As expected, the molecular dynamics (MD) study points out a reduced mobility of the guests within the void space which depends predominantly on the available vacant space [26].

6. $M(CO)_p$ ($p = 5$–3) subcarbonyl species and naked metallic clusters in the void space of M'_nFAU ($n = 0, 56, 85$; $M' = Li^+$, Na^+, K^+, Rb^+, Cs^+)

The sorption of $M(CO)_6$ at room temperature into M'_nFAU zeolites with high aluminum content, causes the partial decarbonylation of $M(CO)_6$ within the void space when n is more than 80 [19,26,59,76–80]. This reaction is found to be faster under gentle thermal treatment and the thermal stability of occluded $M(CO)_6$ increases with the Si/Al ratio. Heating of all the $pM(CO)_6$–M'_nFAU samples results in stepwise decarbonylation of $M(CO)_6$ to naked metallic clusters. A controlled vacuum or reduced CO pressure thermal treatment of the samples provides a mild clean decarbonylation route to yield the corresponding stable subcarbonyl species. ^{129}Xe NMR spectroscopy has proven to be a useful technique in the characterization of the decarbonylation reaction in the void space of Na_{56}FAU [56]. As CO is

removed from the $Mo(CO)_6$–$Na_{56}FAU$ sample by gentle heating under vacuum, the amount of Xe that is adsorbed increases dramatically. In fact, samples containing subcarbonyl species actually adsorb more Xe than bare $Na_{56}FAU$ itself. The enhanced Xe sorption clearly indicates that the subcarbonyl must be located either in the supercages or in the vicinity of the window which connects them.

$$p\mathrm{M(CO)_6}\text{–}\mathrm{M'_nFAU} \rightarrow p\mathrm{M(CO)_3}\text{–}\mathrm{M'_nFAU} + 3p\mathrm{CO}\nearrow \quad (5)$$

The stable $M(CO)_3$ subcarbonyl species (M = Cr, Mo, W) have been studied at high coverage in M'_nFAU ($n = 56$, 85; $M' = Li^+$, Na^+, K^+, Rb^+, Cs^+) by a number of techniques including EXAFS (M = Mo; $M' = Na^+$, Rb^+) [19,23,77], NMR (M = Cr, Mo) [79,80], XPS (M = Mo) [31], UV–visible absorption (Cr, Mo, W), IR absorption spectrometry (Cr, Mo, W) and temperature-programmed decomposition (Cr, Mo, W) etc... The cations effects on the ν(CO) pattern of the $M(CO)_3$–M'_{56} FAU samples demonstrate that the $M(CO)_3$ moiety is anchored with C_s distorted trigonal-pyramidal local symmetry whereas the two exceptions (M = Mo, W; $M' = Cs^+$) exhibit C_{3v} regular trigonal-pyramidal symmetry. From the available experimental results the following conclusions can be obtained [16–19,31,59,67–69]:

(1) The structure of M-subcarbonyl species encaged in Na_{56}- and $Na_{85}FAU$ is described as monomeric $M(CO)_3$ moieties anchored onto the internal surface through M–O(zeolite) linkages with a *fac* configuration.

(2) The M–C bond distance was found to be considerably shorter than those of $M(CO)_3$ complexes, such as $M(CO)_3$(arene). The resultant electron deficient M center of the $M(CO)_3$ moiety is coordinated by the zeolite oxygens. In this respect, zeolite can be regarded as a solid ligand for a $M(CO)_3$ moiety.

(3) The picture of a $M(CO)_3$ moiety migrating by "stepping" from oxide to oxide around the supercage so that the carbonyl orientation is randomized seems plausible. It does not seem likely that the CO ligands could be jumping from metal to metal to produce random orientations because of the long distance of the jumps.

(4) The coordination strength can be easily controlled by varying the zeolite cation, the extent of ion exchange and the Si/Al ratio in the framework. The extent of the $d \rightarrow \pi^*$ electron donation from M to the CO ligands in the grafted $M(CO)_3$ species increases with increasing basicity of zeolite, that is, in the order $M'_{56}FAU < M'_{85}FAU$ and $Li^+ < Na^+ \sim Cs^+$.

The decarbonylation of $pM(CO)_3$–M'_nFAU samples goes to completion under more drastic thermal treatment to yield pM–M'_nFAU samples with occluded naked metallic species in the absence of oxidizing sites ($M' \neq H^+$). The generation and retention of highly dispersed metal clusters in faujasites is subject to several constraints. The interactions between adsorbed carbonyls and the zeolite lattice and cations influence strongly their thermal decomposition and the stability of the resulting species. Recent EXAFS studies of these occluded naked metallic species show that 8 $Mo(CO)_6$–$Rb_{56}FAU$ yields oxygen-framework-stabilized "atomic" molybdenum, whereas fully loaded 16 $Mo(CO)_6$–$Na_{56}FAU$ produces oxygen-framework-stabilized "diatomic" molybdenum [31].

$$p\mathrm{M(CO)_3}\text{–}\mathrm{M'_nFAU} \rightarrow p\mathrm{M}\text{–}\mathrm{M'_nFAU} + 3p\mathrm{CO}\nearrow \quad (6)$$

The Xe uptake for the latter sample is greater than that of $Na_{56}FAU$ containing no metal, indicating that the molybdenum species are present in locations accessible to Xe. Further heat treatment at 623 K cause some of the Xe resonances to move, suggesting that the Mo species may be migrating out of the area accessible to Xe [56].

It should be noted that the UV flash laser photolysis (10 ns) of the 16 $Mo(CO)_6$–$Na_{56}FAU$ sample produces an occluded transient Mo* atom in an excited state through a multiphotonic decarbonylation process. However, the time-resolved Raman spectrometry does not provide evidence for transient small metallic clusters (Mo_2, Mo_3...) over the ns and μs time scales after the laser pulse, besides, the Mo* species probably undergoes cleavage of the CO bond under confinement and subsequent side product formation such as oxocarbures of molybdenum.

The photooxidation of pM(CO)$_6$–$Na_{56}FAU$ samples exposed to gaseous dioxygen produces occluded MoO_3 monomer and W_2O_6 dimer. The photooxidation process is clean and quantitative and is described by the following reaction stoichiometry.

$$p\mathrm{M(CO)_6}\text{–}\mathrm{Na_{56}FAU} + 9/2p\mathrm{O_2} \xrightarrow{h\nu} p\mathrm{MO_3}\text{–}\mathrm{Na_{56}FAU} + 6p\mathrm{CO_2}\uparrow \quad (7)$$

A series of papers have been devoted to the synthesis and study of encapsulated M and MO_3 aggregates. An extensive description of the generation, stabilization and application of such occluded aggregates falls beyond the purpose of the present review.

The IR absorption studies provide evidence of the subcarbonyl species occluded at low coverage in M'_nFAU. The IR spectroscopic behaviors were found to be analogous for M = Cr, Mo, W with small frequency shifts. Particularly, the *in situ* DRIFTS study of the temperature-programmed decomposition of pMo(CO)$_6$–M'_n FAU powdered samples provides some evidence of the formation, nature and thermal stability of the entrapped $Mo(CO)_x$ species through the ν(CO) pattern as functions of the Si/Al ratio and the coverage.

The one-line ν_6 spectrum of the $Mo(CO)_6$–FAU sample was not significantly perturbed by the thermal treatment before the one-step decomposition to metallic aggregates and concomitant desorption which occurs around 430 K [59].

$$\mathrm{Mo(CO)_6}\text{–FAU} \rightarrow \mathrm{Mo}\text{–FAU} + 6\mathrm{CO}\uparrow \quad (8)$$

When the temperature-programmed thermolysis was carried out with the pMo(CO)$_6$–$Na_{56}FAU$ sample under dynamic vacuum, new sets of bands were observed above 360 K, corresponding to the $Mo(CO)_6$–$Na_{56}FAU$ major occluded species with little evidence for appreciable concentration of intermediates. The transient subcarbonyl species were more apparent under CO atmosphere. The thermal evolution of the observed ν(CO) bands depends on the partial pressure of CO even at low pressure, increasing the CO pressure promoted recombination [59].

$$\mathrm{Mo(CO)_6}\text{–}\mathrm{Na_{56}FAU} \rightarrow \mathrm{Mo(CO)_5}\text{–}\mathrm{Na_{56}FAU} + \mathrm{CO} \quad (9)$$

$$\mathrm{Mo(CO)_5}\text{–}\mathrm{Na_{56}FAU} \rightarrow \mathrm{Mo(CO)_4}\text{–}\mathrm{Na_{56}FAU} + \mathrm{CO}\uparrow \quad (10)$$

$$\mathrm{Mo(CO)_4}\text{–}\mathrm{Na_{56}FAU} \rightarrow \mathrm{Mo(CO)_3}\text{–}\mathrm{Na_{56}FAU} + \mathrm{CO}\uparrow \quad (11)$$

A temperature increase above 440 K generates $Mo(CO)_3$. The complete decarbonylation occurred above 550 K according to the following one-step reaction [59].

$$Mo(CO)_3\text{–}Na_{56}FAU \rightarrow Mo\text{–}Na_{56}FAU + 3CO\nearrow \quad (12)$$

When $Mo(CO)_6$ was introduced at relatively low temperature into $Na_{85}FAU$ zeolite, the carbonyl species entrapped is the intact $Mo(CO)_6$ molecule. However, at room temperature the decarbonylation occurs and the ν(CO) DRIFTS spectra provide evidence of the stepwise reversible decarbonylation of $Mo(CO)_6$ (Eqs. (9)–(11)) in the void space of $Na_{85}FAU$ to the stable $Mo(CO)_3$–$Na_{85}FAU$ species which is found to be the major species at 330 K. Heating above 500 K causes the complete disappearance of all the ν(CO) bands and the formation of metallic clusters according to a one-step reaction analogous to Eq. (12).

7. Organization and dynamics of organic ligands (C_6H_6, C_5H_5N, $P(CH_3)_3$) in the void space of M'_nFAU ($n=0, 56, 85$; $M'=Na^+, K^+, Cs^+, H^+$)

7.1. C_6H_6

Powder neutron diffraction has been very successful in elucidating the nature of C_6H_6 sorbed in $Na_{56}FAU$ [42]. At room temperature, the C_6H_6 molecules are largely delocalized within the void space, whereas at 4 K the C_6H_6 molecules are found to be localized on two distinct sites. The first benzene molecule is found in the supercage where it is bonded *via* its π electron density to the SII Na^+ cation. There are four of these sites available per supercage. The second benzene molecule is held by van der Waals forces in the circular 12-membered ring window. There are, on average, two of these sites available per supercage.

At low coverage, the C_6H_6 occupancies are predominantly in front of the SII Na^+ site. At high coverage, the C_6H_6 molecules are found to form molecular clusters at low temperature within the void space. At room temperature, C_6H_6 occupy sites close to their positions at 4 K, they are likely to be performing vigorous molecular motions or are subject to substantial positional disorder. The sorption and dynamic properties of C_6H_6 in zeolites have been investigated experimentally by NMR, QENS (quasi elastic neutron scattering) and INS (inelastic neutron scattering), as well as IR absorption and Raman scattering [81–86].

The heat of sorption of benzene in Na_nFAU, which has been examined by several workers, is known to increase as the Si/Al ratio decreases, presumably reflecting the dominating influence of cation–sorbate interactions [71,72,87]. Benzene mobility has been probed by a variety of techniques, though the disparity between the results obtained from different methods is depressingly large. However, the diffusivity of C_6H_6 is about an order of magnitude higher than that of the xylene isomers. On the other hand, computer simulations back the experimental results because they

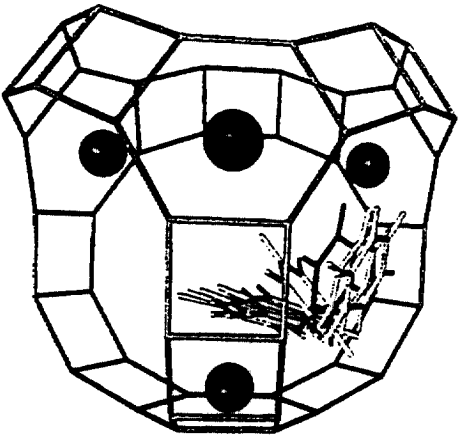

Fig. 5. Predicted SII-window hopping path of C_6H_6 within a $Na_{56}FAU$ supercage. The large spheres represent the Na^+ cations and the shaded cylinders represent the C and H atoms of the C_6H_6 molecule, respectively.

are able to resolve the structure and dynamics of single molecules. Calculations of potential energy maps, energy minimization techniques, MC simulations and MD calculations provide information on static, thermodynamic and dynamic properties. The experimental sorption sites and heat of sorption are in reasonable agreement with the calculated ones [81–87]. Fig. 5

The MD results at room temperature reveal that C_6H_6 is highly mobile in siliceous FAU without demonstrating any particular site preference [82]. At 400 K C_6H_6 becomes more mobile and exhibits cage-to-cage diffusion during the time period of the simulation. For Na_nFAU ($n=56$, 85) the diffusion is found to be two orders of magnitude slower than in FAU, ~200 ns would be required to observe cage-to-cage motion (~2 nm) [81]. Within the supercage the predominant rotational motion is the rotation about the six-fold axis in accurate agreement with QENS studies. The diffusional mechanism can be described as a jump model with residential probability at the cation sorption site in accurate agreement with NMR studies. The vibrational spectroscopies provide a direct evidence of the mobility of C_6H_6 within Na_nFAU in the time scale of the vibration phenomenon.

7.2. C_5H_5N

Spectroscopic studies have used basic probe molecules, such as pyridine (C_5H_5N) for which there is a clear distinction between the protonated cation and the neutral molecules to explore the nature of the acids sites in zeolites. Hence, IR absorption studies on C_5H_5N adsorbed in H_nFAU and Na_nFAU zeolites show the formation of pyridinium ions and therefore, the dominance of Brönsted sites in the former, and suggest adsorption at the Lewis site in the latter. Similar indications obtained by ^{15}N NMR spectroscopy have supported this conclusion. The direct

evidence for the location of C_5H_5N in $Na_{56}FAU$ has come from a powder neutron diffraction study [88]. C_5H_5N sorbed at low coverage in $Na_{56}FAU$ has been located in the window. However, the spectroscopic studies show that C_5H_5N is also adsorbed at a Lewis acid site, which may be associated with the charge balancing Na^+ cation. The main trends of the sorption of pyridine in faujasitic zeolites appear to be analogous to those reported for benzene sorption.

7.3. $P(CH_3)_3$

^{31}P MAS-NMR, ^{23}Na MAS-DOR-NMR and IR absorption spectroscopic analysis of $mP(CH_3)_3$–$Na_{56}FAU$ favors a scheme in which each $P(CH_3)_3$ is coordinated to a site Na^+ cation. At saturation loading it is therefore likely that the four $P(CH_3)_3$ molecules are sorbed to the four tetrahedrally disposed site II Na^+ cations. The additional $P(CH_3)_3$ molecules probably reside in the vicinity of the four 12-ring entrance windows [25].

8. Organization, dynamics and cooperative effects of $M(CO)_6$ and C_6H_6 or C_5H_5N, or $P(CH_3)_3$) cosorbed in Na_nFAU ($n=0$, 56, 85)

8.1. $M(CO)_6$–C_6H_6

Firstly, we present DRIFTS investigations and Monte Carlo simulations of the cosorption of $Mo(CO)_6$ and benzene in faujasitic zeolites Na_nFAU ($n=0$, 56, 85). Upon sorption of C_6H_6 (15–30 C_6H_6–FAU) in the presence of $Mo(CO)_6$ (0.1–0.5 $Mo(CO)_6$–FAU) additional bands are observed in the wave number ranges of the vibrational modes of benzene. The similarity between the IR spectra of C_6H_6 in solution, sorbed and cosorbed in FAU provides evidence that the C_6H_6 molecules within the porous voids approach, at room temperature, the rapid limit characteristic of a liquid. Upon sorption in FAU the IR spectrum of benzene hardly changes as the benzene loading increases. According to previous experiments [17–19], the bands observed at 1960 and 1820 cm^{-1} are assigned to combination modes of out-of-plane bending modes γ(C–H) whereas the intense band at 1478 cm^{-1} is assigned to the fundamental $\nu_{19}(E_{1u})$ stretching mode ν(C–C). After subtraction from the cosorbed sample spectrum of the spectrum of benzene sorbed alone, the remaining one-band spectrum is found to be analogous to the spectrum of $Mo(CO)_6$ sorbed alone in the FAU zeolite, except for a weak frequency shift. A random distribution of both the $Mo(CO)_6$ and benzene molecules within the porous void of siliceous FAU is postulated subsequently [27].

Upon adsorption of C_6H_6 (16–30 C_6H_6–$Na_{56}FAU$) in the presence of $Mo(CO)_6$ (0.1–0.5 $Mo(CO)_6$–$Na_{56}FAU$) additional bands are observed in the vibration regions of the C_6H_6 molecule. These bands are in correct agreement with previously reported data concerning benzene sorbed alone in $Na_{56}FAU$ zeolite [18]. Particularly, the shape of the bands progressively changes as the benzene loading

increases. The two pairs of IR bands 2013/1880 and 1983/1847 cm^{-1} corresponding to the out-of-plane γ(C–H) combination modes were used previously to characterize the benzene adsorption sites [18]. The high-frequency pair 2013/1880 cm^{-1} is related to the benzene sorbed in the 12-ring window whereas the lower-frequency pair 1983/1847 cm^{-1} arises from benzene with the Na^+ cations in site II [18]. The preference for SII Na^+ cations mentioned above is detected at low C_6H_6 loadings, the adsorption in the 12-ring window starting to increase significantly only after 20 C_6H_6 per unit cell are sorbed. It should be noted that other cationic faujasites may give a different order of preferred adsorption [18]. After subtraction from the DRIFTS pattern (cosorbed samples) of the spectrum of benzene (singly sorbed sample) the remaining spectrum does not correspond to the spectrum of $Mo(CO)_6$ sorbed alone in the Na_{56}FAU zeolite. The DRIFTS spectra indicate significant frequency shifts and relative IR intensity changes of the ν(CO) modes upon cosorption of benzene. It is postulated that the presence of benzene in the porous void generates a new sorption site for $Mo(CO)_6$ with C_6H_6 molecules in close proximity.

Upon sorption at 250 K of C_6H_6 (16–30 C_6H_6–Na_{85}FAU) in the presence of $Mo(CO)_6$ sorbed at 250 K (0.1–0.5 $Mo(CO)_6$–Na_{85}FAU) additional bands are observed in the fundamental vibration regions of the C_6H_6 molecule. The IR bands of C_6H_6 are found to be analogous to those observed previously for benzene sorbed alone in Na_{85}FAU. The pair of bands observed at 1866 and 1847 cm^{-1} is found to be typical of two types of adsorption sites for benzene [17]. However, the distribution of benzene between the two modes of sorption, cations and 12-ring windows is strongly directed by the chemical properties of the zeolite. After subtraction from the DRIFTS pattern (cosorbed sample) of the DRIFTS spectrum of benzene (singly sorbed sample), the remaining ν(CO) spectrum is found to be analogous to the spectrum of $Mo(CO)_6$ sorbed alone in the Na_{85}FAU zeolite at 250 K. The DRIFTS spectra indicate no significant frequency shifts and relative IR intensity changes of the ν(CO) modes upon cosorption of benzene. It is postulated that the sorptions of $Mo(CO)_6$ and benzene occur in different domains of the porous void of Na_{85}FAU.

The fact that no significant cosorption was obtained with bulky arenes such as 1,3,6-tris(*tert*-butyl)benzene demonstrates the exclusive free access to the porous void of the small arenes [19,27].

The DRIFTS spectroscopic results are supported by grand canonical Monte Carlo (GCMC) simulations of the cosorption of $Mo(CO)_6$ and C_6H_6 at constant pressures. The pressure values were adjusted to approximately mimic the experimental coverages. The conditions of the simulations have been given in previous works [27]. The validity of the set of parameters used throughout the present article is given by the possibility to reasonably reproduce the experimental C_6H_6 loadings in Na_nFAU (n= 0, 56, 96) [18] and the siting locations of C_6H_6 in Na_{56}FAU [16,23]. In addition, the predicted $Mo(CO)_6$ siting locations are in close agreement with the spectroscopic behavior of $Mo(CO)_6$ occluded in Na_nFAU (n=0, 56, 85) [27].

The prediction of C_6H_6–$Mo(CO)_6$ cosorption in siliceous FAU was carried out at 300 K and the constant pressures were adjusted to correspond approximately to the respective experimental loadings. In the presence of C_6H_6 at high pressure, no

$Mo(CO)_6$ cosorption was simulated and all the porous volume is filled with C_6H_6 molecules (32 C_6H_6–FAU). At lower C_6H_6 pressures the suitable loadings are found to be 1 $Mo(CO)_6$ and 25 C_6H_6 per unit cell and the corresponding sorption energies are found to be -7.0 and -10.6 kcal mol^{-1}, respectively. The distribution of positions occupied by $Mo(CO)_6$ and C_6H_6 is large. The absence of well-defined sorption sites indicates that the net potential surface accessible to the molecules is fairly uniform. These results are in close agreement with the isotropic behavior observed from DRIFTS experiments.

From accurate starting pressure values, the GCMC simulations of C_6H_6–$Mo(CO)_6$ cosorption in Na_{56}FAU provide loadings in reasonable agreement with the experimental values used in the DRIFTS experiments, 1 or 2 $Mo(CO)_6$ and 30 C_6H_6 per unit cell, respectively. At high C_6H_6 pressures, the corresponding sorption energy is found to be -10 kcal mol^{-1} for $Mo(CO)_6$ and -11 kcal mol^{-1} (window) and -19 kcal mol^{-1} (cation) for C_6H_6, respectively. It should be noted that similar energy values are reproduced for C_6H_6 during the simulation of the sorption of C_6H_6 alone [23]. The distribution of positions occupied by $Mo(CO)_6$ according to the -10 kcal mol^{-1} energy is located within the cavity, whereas C_6H_6 molecules lie in the same cavity facially coordinated to the SII cations (-19 kcal mol^{-1}) or centered in the window (-11 kcal mol^{-1}). The presence of C_6H_6 molecules in the porous voids stabilizes the $Mo(CO)_6$ location within the supercage rather than in the window as predicted by the MC simulations of the sorption of $Mo(CO)_6$ alone. In the case of cosorption when the average $Mo(CO)_6$ loading is more than two molecules per unit cell, some supercages are occupied by 2 $Mo(CO)_6$. The sorption energies of the benzene occluded alone in Na_{56}FAU or cosorbed with $Mo(CO)_6$ are analogous whereas the sorption energy of $Mo(CO)_6$ at low coverage is found to be markedly lower than cosorbed with benzene at high coverage, -12 and -10 kcal mol^{-1}, respectively. The siting locations of the C_6H_6 and $Mo(CO)_6$ molecules are in good agreement with the DRIFTS data and the spectral changes observed in the ν(CO) region reflect the $Mo(CO)_6$ siting location change during the cosorption of benzene into the Na_{56}FAU zeolite. Fig. 6

From accurate starting pressure values, the GCMC simulations at 250 K of the C_6H_6–$Mo(CO)_6$, Na_{85}FAU cosorption provide a loading, corresponding to the sorption of 38 C_6H_6 per unit cell. There is no cosorption of $Mo(CO)_6$ in the presence of benzene after equilibration of the system. The corresponding sorption energies are found to be -12 and -17 kcal mol^{-1} for C_6H_6. The C_6H_6 molecules are facially coordinated to the SII and SIII cations in the supercage (-17 kcal mol^{-1}) or in the vicinity of the windows (-12 kcal mol^{-1}). Analogous energy values concerning the sorption of C_6H_6 in Na_{85}FAU were reported earlier [21]. The sorption energy of $Mo(CO)_6$ occluded alone in Na_{96}FAU at constant coverage was found previously to be -9 kcal mol^{-1} [37]. Before the saturation of the porous volume by the C_6H_6 molecules, the occluded $Mo(CO)_6$ molecules observed during the DRIFTS experiments (see above) are probably located in domains without any benzene molecule in close proximity [86].

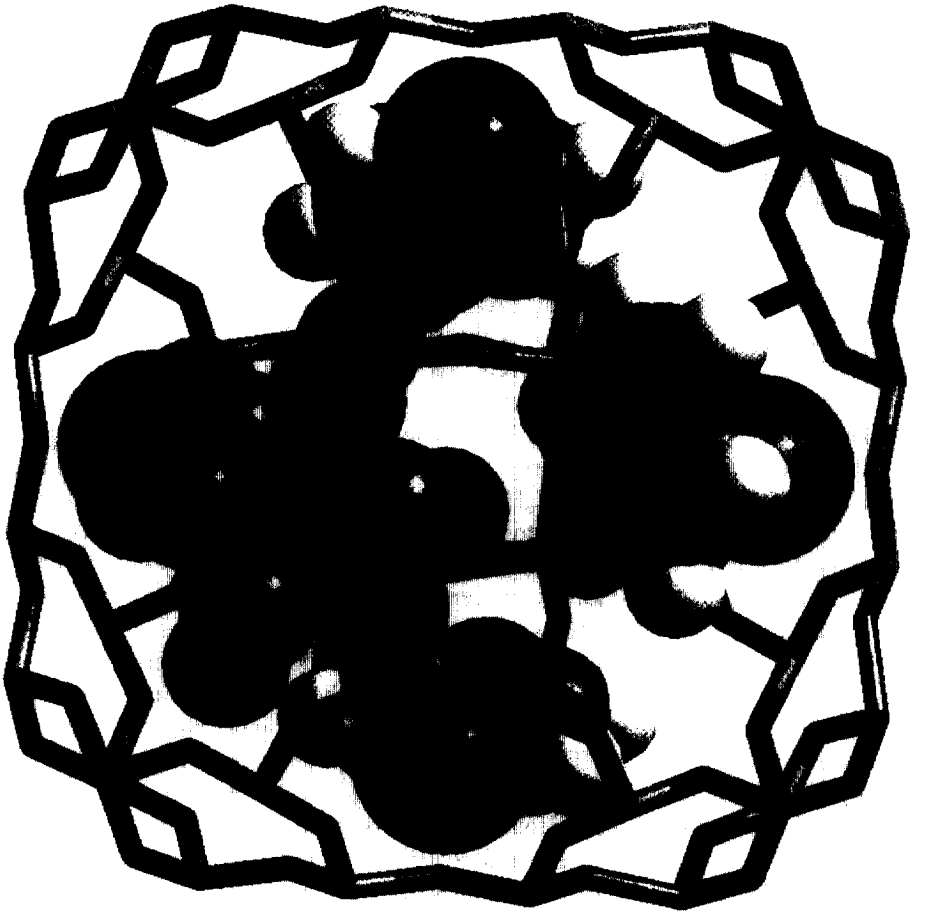

Fig. 6. Predicted sorption sites of $Mo(CO)_6$ and C_6H_6 in $Na_{56}FAU$ (1 $Mo(CO)_6$, 30 C_6H_6/unit cell). The black and shaded cylinders represent O and Si/Al atoms of the zeolite framework, respectively. The shaded and white spheres represent C and H atoms of C_6H_6, respectively. The large spheres represent Na^+, the medium black and shaded spheres represent O and C atoms of $Mo(CO)_6$, respectively.

8.2. $M(CO)_6$–C_5H_5N

Upon sorption of C_5H_5N in $Na_{56}FAU$ in the presence of $Mo(CO)_6$ additional bands are observed in the vibration regions of the C_5H_5N molecule. These bands are in correct agreement with previously reported data concerning pyridine sorbed alone in the $Na_{56}FAU$ zeolite. After subtraction from the DRIFTS pattern (cosorbed samples) of the spectrum of C_5H_5N (singly sorbed sample) the remaining spectrum does not correspond to the spectrum of $Mo(CO)_6$ sorbed alone in the $Na_{56}FAU$ zeolite. The DRIFTS spectra indicate significant frequency shifts and relative IR intensity changes of the ν(CO) modes upon cosorption of C_5H_5N. It is postulated that the presence of C_5H_5N in the porous void generates a new sorption site for

$Mo(CO)_6$ with C_5H_5N molecules in close proximity. However, at high C_5H_5N coverage, the ν(CO) bands disappear progressively and provide evidence of the desorption of $Mo(CO)_6$ upon sorption of C_5H_5N at high coverage [86].

8.3. $M(CO)_6$–$P(CH_3)_3$

The sorption of $P(CH_3)_3$ in Na_{56}FAU in the presence of $Mo(CO)_6$ induces a partial collapse of the six-line ν(CO) IR spectrum [25]. The resulting ν(CO) spectrum (4$Mo(CO)_6$, 16 $P(CH_3)_3$–Na_{56}FAU) is characteristic of $Mo(CO)_6$ which at room temperature approaches the characteristics of a liquid. The cation translatory modes of Na^+ found in the far-IR spectra show small but reproducible frequency shifts and intensity changes following occlusion of $Mo(CO)_6$, annealing and addition of $P(CH_3)_3$. The $P(CH_3)_3$ effect is interpreted in terms of a type of deannealing process of the $Mo(CO)_6$ guest induced by $P(CH_3)_3$–Na^+ interactions. Strong evidence of the cooperative effects within the supercage was provided by the DOR-MAS-NMR spectra of the 4 $Mo(CO)_6$, 16 $P(CH_3)_3$–Na_{56}FAU sample. The results provide compelling evidence for a direct electronic effect exerted by the $P(CH_3)_3$ on the site II Na^+ in interaction with $Mo(CO)_6$.

9. Investigations of the intrazeolite reactions between $M(CO)_6$ and ligands (C_6H_6, C_5H_5N, $P(CH_3)_3$) in Na_nFAU ($n = 0, 56, 85$). Identification of the reaction products within the zeolitic porous space

9.1. $M(CO)_6$–C_6H_6

During the thermal treatment, under 1 atm of helium, of the 0.5 $Mo(CO)_6$, 20 C_6H_6–FAU loaded zeolite no significant changes were observed in the shapes of the DRIFTS spectra except the progressive disappearance of the intense band assigned to the ν_6(CO) mode of $Mo(CO)_6$. The disappearance of the ν_6(CO) band corresponds to the desorption of $Mo(CO)_6$ upon thermolysis before any reaction in the void space of the FAU zeolite. At 500 K, only C_6H_6 was detected in the internal volume of the zeolite. The $Mo(CO)_6$ departure from the zeolite framework to the gas phase was controlled by IR absorption spectroscopy.

During the thermal treatment of the 2 $Mo(CO)_6$, 30 C_6H_6–Na_{56}FAU loaded zeolite, heating above 320 K again causes a dramatic change in the ν(CO) set of bands whereas the C_6H_6 set of bands remain unaffected in the experimental (73–500 K) temperature range. The transformation appears to go to completion at 423 K over less than 0.5 h in the experimental conditions. After subtraction from the resulting DRIFTS pattern of the DRIFTS bands of benzene the new ν(CO) set of bands are found to be analogous to those observed for $Mo(CO)_3(\eta^6\text{-}C_6H_6)$ occluded alone in Na_{56}FAU. It should be noted that the zeolite was loaded with $Mo(CO)_3(\eta^6\text{-}C_6H_6)$ through immersion into the pentane solution and subsequent evaporation of the solvent because of the poor vapor pressure of the organometallic

compound which does not allow any vapor phase transfer into the zeolite at room temperature.

The three ν(CO) bands observed at 1948, 1857 and 1832 cm^{-1} do not correspond to any intrazeolite $Mo(CO)_n$ ($n=3$, 4, 5) subcarbonyl species [27,59]. The three ν(CO) bands derived from the A_1 and E modes of the $Mo(CO)_3(\eta^6\text{-}C_6H_6)$ free molecule indicate that the local symmetry is low in the sorption site. In practice one finds that the reaction of 2 $Mo(CO)_6$ with 30 C_6H_6 in Na_{56}FAU cleanly yields $Mo(CO)_3(\eta^6\text{-}C_6H_6)$ as a product according to the following intrazeolitic reaction [19,27].

$$2Mo(CO)_6,\ 30C_6H_6\text{–}Na_{56}FAU \rightarrow 2Mo(CO)_3(\eta^6\text{-}C_6H_6),\ 28C_6H_6\text{–}Na_{56}FAU + 6CO\uparrow \quad (13)$$

This intrazeolitically generated complex can be considered to form by capping the tricarbonyl moiety with the benzene ligand [19]. Identical DRIFTS results are observed when an excess of benzene is introduced into the cell after partial decarbonylation reaction under thermolysis at 440 K. The intrazeolitic reaction of the subcarbonyl $Mo(CO)_3$–Na_{56}FAU with C_6H_6 yields as a product $Mo(CO)_3(\eta^6\text{-}C_6H_6)$ according to the following intrazeolitic reaction.

$$Mo(CO)_3\text{–}Na_{56}FAU + 20C_6H_6 \rightarrow Mo(CO)_3(\eta^6\text{-}C_6H_6),\ 19C_6H_6\text{–}Na_{56}FAU \quad (14)$$

An analogous behavior was reported for the 1,3,5-cycloheptatriene as ligand in Na_{56}FAU, to yield the occluded $Mo(CO)_3(\eta^6\text{-}1,3,5\text{-}C_7H_8)$ complex [19]. No attempt to obtain quantitative kinetic information about the intrazeolitic reaction between $Mo(CO)_6$ and C_6H_6 in Na_{56}FAU has been undertaken yet. However, the reaction rate is found to be strongly dependent on the extent of loading of $Mo(CO)_6$ and C_6H_6 and on the CO gas pressure. The effects of these parameters on intrazeolitic organometallic reaction rates have been quantitatively evaluated recently in the case of the reaction between $Mo(CO)_6$ and $P(CH_3)_3$ [25]. Particularly, after an equilibrium period (300 K), at low and quite constant $Mo(CO)_6$ coverage, the reaction rate (400 K) increases slightly with increasing C_6H_6 loading in the experimental range (15–30 C_6H_6/unit cell). Whereas at constant C_6H_6 coverage, the reaction rate remains approximately constant with increasing $Mo(CO)_6$ loading over the range 0.02–1 $Mo(CO)_6$/unit cell. Then, the reaction rate shows a significant decrease at higher $Mo(CO)_6$ loading. In addition, under dynamic vacuum the reaction appears faster than under static helium atmosphere. The amount of CO released during the reaction may be sufficient to increase the rate substantially in Na_{56}FAU.

During the thermal treatment of the 1 $Mo(CO)_6$, 30 C_6H_6–Na_{85}FAU sample obtained at 270 K, heating above 300 K caused a dramatic change in the DRIFTS patterns. After subtraction from the DRIFTS pattern of the benzene spectrum in Na_{85}FAU, the resulting ν(CO) set of bands exhibit clearly the spectral characteristics of several anchored subcarbonyl species ($Mo(CO)_x$, $x=3$–6) [59]. Near 500 K a two-line spectrum is predominantly observed at 1912 and 1775–1750 cm^{-1}. This set

of ν(CO) bands was attributed previously to the intrazeolitic $Mo(CO)_3$–$Na_{85}FAU$ species [76]. The DRIFTS experiments provide no evidence of the intrazeolitic $Mo(CO)_3(\eta^6\text{-}C_6H_6)$–$Na_{85}FAU$ species. In addition, heating above 500 K provokes the one-step decomposition of $Mo(CO)_3$ before any reaction with the benzene molecules [27].

With bulky arenes, no supplementary species was observed under the same experimental conditions except the occluded $M(CO)_{6-x}$ subcarbonyl species ($x=1$, 2, 3). The outer surface does not participate significantly to the reaction yield.

9.2. $M(CO)_6$–C_5H_5N

The stoichiometric mechanisms of the reactions of $Mo(CO)_6$ with C_5H_5N in the void space of $Na_{56}FAU$ are established by the DRIFTS investigation of the thermal activation of $Mo(CO)_6$, C_5H_5N–$Na_{56}FAU$ cosorbed samples and through the comparison of the corresponding IR absorption spectra of $Mo(CO)_{6-x}(C_5H_5N)_x$ ($x=1$, 2, 3) obtained in solution. Under thermal activation at 420 K $Mo(CO)_3(C_5H_5N)_3$ is the only product detected by DRIFTS in the absence of CO [86].

$$Mo(CO)_6,\ 30C_5H_5N\text{–}Na_{56}FAU$$

$$\rightarrow Mo(CO)_3(C_5H_5N)_3,\ 27C_5H_5N\text{–}Na_{56}FAU + 3CO\nearrow \quad (15)$$

Applied reduced pressures of CO generate $Mo(CO)_4(C_5H_5N)_2$ and $Mo(CO)_5(C_5H_5N)$ intermediates and finally regenerate $Mo(CO)_6$.

9.3. $M(CO)_6$–$P(CH_3)_3$

The stoichiometric mechanisms of the reactions of $Mo(CO)_6$ in the void space of $M'_{56}FAU$ zeolites with $P(CH_3)_3$ are established by the analysis of the extensive data presented in previous work [25]. Reactions with $P(CH_3)_3$ are inhibited by CO in accordance with the sequence of reactions shown in Eqs. (9), (10) and (16).

$$Mo(CO)_4\text{–}Na_{56}FAU + 2P(CH_3)_3 \rightarrow cis\text{-}Mo(CO)_4[P(CH_3)_3]_2\text{–}Na_{56}FAU \quad (16)$$

The sequence of reactions shown in Eqs. (9), (10) and (16) is also supported by the fact that *cis*-$Mo(CO)_4[P(CH_3)_3]_2$ is the only product in the absence of CO. Substitution by $P(CH_3)_3$ is retarded by applied pressures of ^{12}CO, as expected, but it is also retarded to a significant extent by increased $Mo(CO)_6$ and $P(CH_3)_3$ loadings. Substitution by ^{13}CO is similarly retarded by increasing pressures of entering ^{13}CO. This behavior can be interpreted on the basis of structural information concerning pertinent reactant and product guests obtained from several techniques.

As in homogeneous solution, reactions proceed by CO-dissociative paths and, with the strong nucleophile $P(CH_3)_3$, by associative paths. The rate of the dissociative path is accelerated at 340 K by ca. 10^3 compared with the rate in homogeneous solution. The probabilities of the associative paths are significantly greater in zeolite

than in homogeneous solution but these paths are not appreciably affected by different loading of $Mo(CO)_6$ or $P(CH_3)_3$ or by different applied pressures of CO.

The best model that emerges from this study pictures a supramolecular assembly of $Mo(CO)_6$ and $P(CH_3)_3$ and CO houses within the void space, subject to loading-dependent cooperative interactions. These interactions appear to control the extent of activation of $Mo(CO)_6$ through the degree of ordering of the dissociative $\{Mo(CO)_5...CO\}^*$ transition state [25].

10. Energetics and sorption sites of the reaction products in the zeolitic porous space

The intrazeolitic generated complexes were convincingly identified by comparing their mid-IR absorption spectra in the ν(CO) region with those independently obtained through sublimation or impregnation of $M(CO)_3(\eta^6\text{-}C_6H_6)$, $Mo(CO)_3(\eta^6\text{-}1,3,5\text{-}C_7H_8)$. Particularly, the set of three ν(CO) bands corresponds to a $Mo(CO)_3(\eta^6\text{-}C_6H_6)$ or $Mo(CO)_3(\eta^6\text{-}1,3,5\text{-}C_7H_8)$ molecule located in a site with low local symmetry [19]. However, the ν(CO) stretching frequencies are shifted toward lower energies compared to the respective solution phase values. In addition, the supplementary splitting or broadening of the bands, which occur at higher coverage, can be attributed to the two different types of sorption sites and vibrational intermolecular coupling. The intrazeolitic generated complexes are obtained with an excess of ligand which can change the location site of the complex and change somewhat the IR absorption spectra.

The DRIFTS spectroscopic results concerning the intrazeolitic generated and sorbed $Mo(CO)_3(\eta^6\text{-}C_6H_6)$ complex are supported by both canonical Monte Carlo (MC) at fixed loading and grand canonical Monte Carlo (GCMC) simulations at fixed pressures. The pressure values were adjusted to approximately mimic the experimental coverages. The conditions of the simulations have been given in previous work [27].

The prediction of the $Mo(CO)_3(\eta^6\text{-}C_6H_6)$ sorption and $Mo(CO)_3(\eta^6\text{-}C_6H_6)\text{–}C_6H_6$ cosorption was carried out at 300 K and at fixed pressures. In the presence or in the absence of C_6H_6, the distribution of positions occupied by $Mo(CO)_3(\eta^6\text{-}C_6H_6)$, in the vicinity of the window, is found to be large. The absence of well-defined sorption sites indicates that the net potential surfaces accessible to the molecules are fairly uniform. These results are consistent with the isotropic behavior of $Mo(CO)_3(\eta^6\text{-}C_6H_6)$ in FAU observed from DRIFTS experiments. No further investigation has been undertaken yet, because this subject falls beyond the scope of this work. Indeed no intrazeolitic reaction between $Mo(CO)_6$ and C_6H_6 is detected before the desorption of $Mo(CO)_6$ (see above).

Firstly, the MC simulations of the sorption of $Mo(CO)_3(\eta^6\text{-}C_6H_6)$ into $Na_{56}FAU$ were carried out at 300 K and at a fixed loading. In this case the sorbate–sorbate interactions do not take place. The $Mo(CO)_3(\eta^6\text{-}C_6H_6)$ molecule lies inside the supercage, the C_6H_6 moiety is facially coordinated to the SII Na^+ cation. However, 95% of the center of mass sampled during the simulations is located within an isosurface of the probability density of the molecule, the three lobes are oriented

to the three remaining SII cations of the supercage, respectively. They represent the equal probability for each CO ligand to be in close proximity to a SII cation. Fig. 7

The prediction of sorption of $Mo(CO)_3(\eta^6\text{-}C_6H_6)$ at higher filling was carried out at constant pressure. The average calculated loading corresponding to the filling of the voids was found to be 19 $Mo(CO)_3(\eta^6\text{-}C_6H_6)$ per unit cell. The contoured regions of the distribution of positions of the center of mass provide clear evidence of two types of sorption sites. The first one corresponds to the SII Na^+ facially coordinated C_6H_6 moiety and the second one to the C_6H_6 moiety centered in the 12-ring window. The ratio of the population of the sites depends on the filling, particularly at high loading the confinement of the molecules in the porous void constrains the molecules to reside preferentially near the windows through intermolecular contacts. This sorption model appears to be in reasonable agreement with

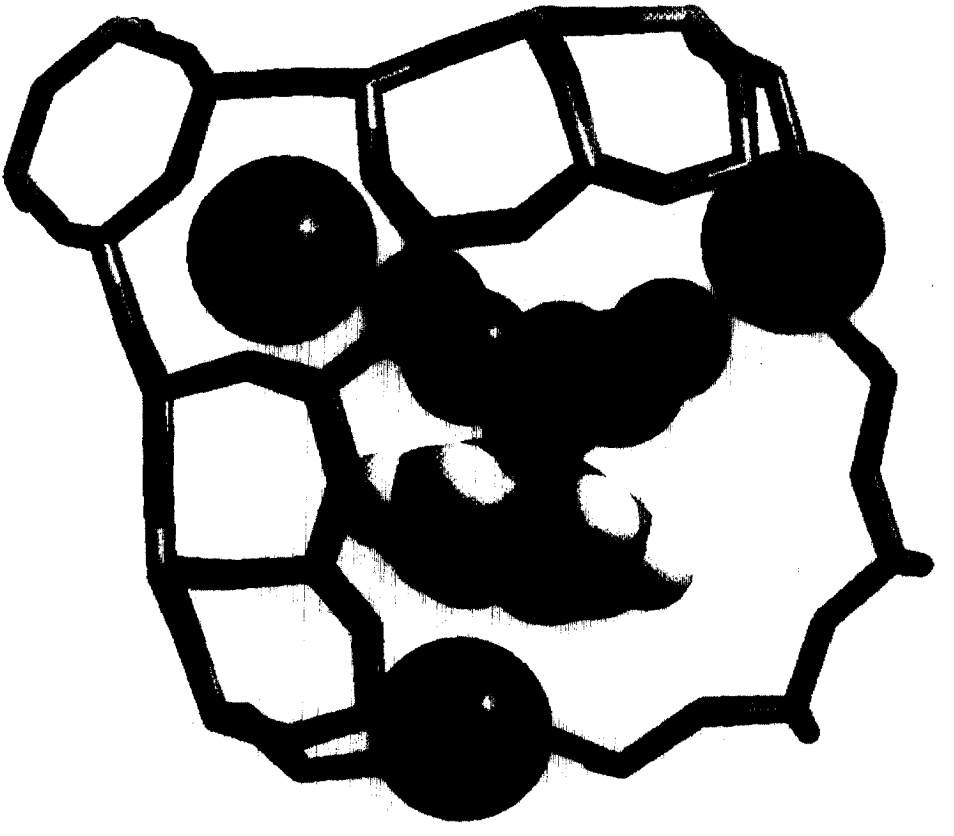

Fig. 7. Probable location of $Mo(CO)_3(\eta^6\text{-}C_6H_6)$ in the $Na_{56}FAU$ supercage at low coverage (1 $Mo(CO)_3(\eta^6\text{-}C_6H_6)$/unit cell). The black and shaded cylinders represent O and Si/Al atoms of the zeolite framework, respectively. The shaded and white spheres represent the C and H atoms of C_6H_6, respectively. The large shaded spheres represent Na^+, the medium black and shaded spheres represent O and C atoms of $Mo(CO)_6$, respectively.

the previous and present IR spectroscopic data concerning $Mo(CO)_3(\eta^6\text{-}C_6H_6)$ as well as parent complexes sorbed alone.

The GCMC simulations of the $Mo(CO)_3(\eta^6\text{-}C_6H_6)$–$C_6H_6$ cosorption are directly related to the *in situ* DRIFTS study of the intrazeolitic reaction between $Mo(CO)_6$ and C_6H_6 cosorbed in $Na_{56}FAU$. From accurate starting pressure values, the GCMC simulations provide loadings in reasonable agreement with the experimental values used in the DRIFTS experiments, 2 $Mo(CO)_6$ and 28 C_6H_6 per unit cell, respectively. The distribution of positions occupied by $Mo(CO)_3(\eta^6\text{-}C_6H_6)$ according to the -21 kcal mol^{-1} energy is located within the cavity, whereas the C_6H_6 molecules are facially coordinated to the SII cations in the supercage (-19 kcal mol^{-1}) or centered in the window (-11 kcal mol^{-1}). The C_6H_6 moiety of the $Mo(CO)_3(\eta^6\text{-}C_6H_6)$ molecule is facially coordinated to the SII Na^+ cation.

No attempts to study the dynamic processes of occluded $M(CO)_3(C_6H_6)$ have been undertaken, yet. However, from proton relaxation studies and potential energy barrier calculations for $M(CO)_3$(arene) in the bulk state, it is probable that the arene group is able to rotate freely at room temperature, whereas $(CO)_3$ reorientation encounters a larger energy barrier [89,90]. Fig. 8

The presence of C_6H_6 molecules in the void space does not markedly modify the siting site preference predicted by the MC simulations of the sorption of the $Mo(CO)_3(\eta^6\text{-}C_6H_6)$ molecule alone. The sorption energies of the benzene sorbed alone in $Na_{56}FAU$ or cosorbed with $Mo(CO)_3(\eta^6\text{-}C_6H_6)$ are analogous whereas the

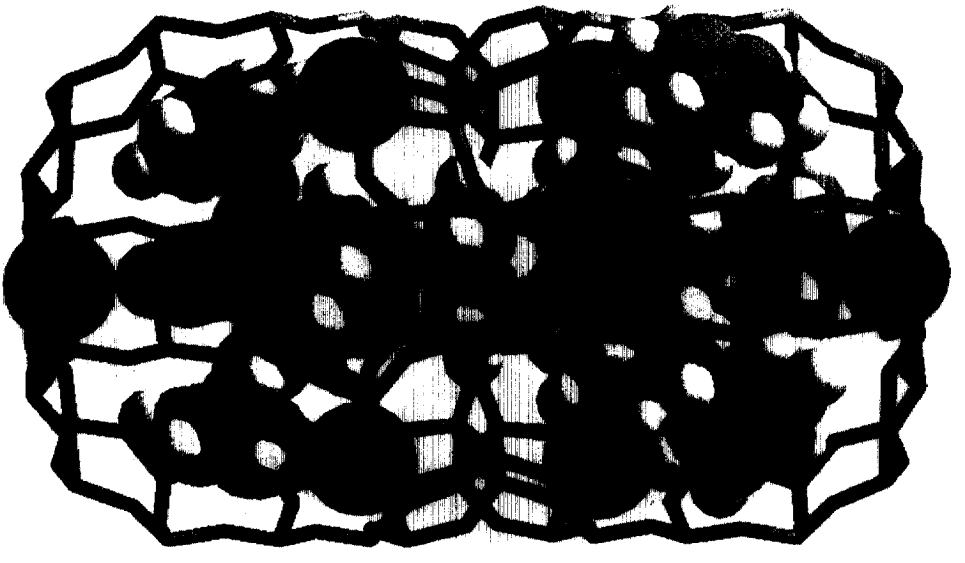

Fig. 8. Predicted sites of $Mo(CO)_3(\eta^6\text{-}C_6H_6)$ and C_6H_6 cosorbed in $Na_{56}FAU$ (1 $Mo(CO)_3(\eta^6\text{-}C_6H_6)$, 30 C_6H_6/unit cell). Two supercages of zeolite $Na_{56}FAU$ and the interconnecting 12-ring window. The black and shaded cylinders represent O and Si/Al atoms of the zeolite framework, respectively. The shaded and white spheres represent the C and H atoms of C_6H_6, respectively. The large shaded spheres represent Na^+, the medium black and shaded spheres represent O and C atoms of $Mo(CO)_6$, respectively.

energy of $Mo(CO)_3(\eta^6\text{-}C_6H_6)$ sorbed alone at low coverage is found to be slightly higher than cosorbed with benzene at high coverage, -20 and -21 kcal mol^{-1}, respectively. The siting locations of the C_6H_6 and $Mo(CO)_3(\eta^6\text{-}C_6H_6)$ molecules appear to be in close agreement with the DRIFTS data. Particularly, the weak changes observed between the ν(CO) sets, reflect an analogous siting location for $Mo(CO)_3(\eta^6\text{-}C_6H_6)$ sorbed alone or cosorbed with C_6H_6 in the Na_{56}FAU zeolite.

The MC simulations of the sorption of $Mo(CO)_3(\eta^6\text{-}C_6H_6)$ into Na_{85}FAU were carried out at 300 K at fixed loading and at fixed pressure. The results were reported recently and fall out of the scope of this review because $Mo(CO)_3(\eta^6\text{-}C_6H_6)$ cannot be obtained through Na_{85}FAU intrazeolite reactions [27].

11. Reaction pathways between $M(CO)_6$ (M = Cr, Mo, W) and ligands within the void space of faujasitic zeolites. Conclusions

Treatment of metal carbonyls such as $M(CO)_6$ with ligands such as arenes in solution may give arene metal carbonyl complexes. Irradiation with ultraviolet light assists the reaction, or it may be more effective to carry out the reaction in a high-boiling, coordinating solvent such as diglyme ($CH_3OCH_2CH_2OCH_2CH_2OCH_3$) [27]. The role of the coordinating solvent was found to accelerate the dissociation of $M(CO)_6$ which is found to be slow.

It is known that $M(CO)_6$ can react thermally in the void space of zeolites in the absence of added reagents even at room temperature. The main conclusions can be summarized as follows: The faujasitic zeolites with high aluminum content (Si/Al = 1.26) promote an easy sequential decomposition of $M(CO)_6$ at room temperature. The loss of three CO ligands of $M(CO)_6$ forms a moiety in which the three coordination sites thus made vacant are occupied by framework oxygens acting as a zeolate ligand [31]. The subcarbonyl species are stabilized through the significant Lewis basicity (electron density) of the framework oxygens [28,35]. The basicity of the oxygen, measured through the charge density, decreases concomitantly with the aluminum content of the zeolite framework. The Na_{56}FAU framework (Si/Al = 2.5) reduces the stabilization of the subcarbonyl species and increases the intrazeolite decomposition temperature of $M(CO)_6$ [36]. The $M(CO)_6$ thermal behavior in siliceous faujasite FAU (Si/Al = 100) is found to be analogous to that observed in polyether solvents where no discrete subcarbonyl species are detected. In summary, a significant basicity of the framework oxygens prevents the recombination reactions of the subcarbonyl species with CO inside the void space.

From the extensive quantitative kinetic study of the thermal reaction between $Mo(CO)_6$ and trimethylphosphine $P(CH_3)_3$ encapsulated in Na_{56}FAU to form $Mo(CO)_4(P(CH_3)_3)_2$, the effects of $P(CH_3)_3$, $Mo(CO)_6$ loadings and CO pressure on the rate of the substitution reactions have been evaluated [25]. The substitution reactions of $Mo(CO)_6$ with $P(CH_3)_3$ within the void space of the Na_{56}FAU host proceed by pseudo-first-order dissociative and associative processes.

Analogous trends have been found for the substitution reactions of $Mo(CO)_6$ with C_6H_6 within the void space of the Na_nFAU hosts ($n = 0$, 56, 85). Dissociative

substitution of $Mo(CO)_6$ by C_6H_6 is accelerated through evacuation of CO under vacuum or retarded to a significant extent by increased CO pressure as $Mo(CO)_6$ and C_6H_6 loading. The reactions between $Mo(CO)_6$ and C_6H_6 to form $Mo(CO)_3(\eta^6\text{-}C_6H_6)$ within the void space of $Na_{56}FAU$ (Si/Al = 2.5) occur at lower temperature and are faster than the corresponding reactions in homogeneous solution. However, the present experiments point out the important role of the nature of the faujasitic zeolite towards the substitution reactions under study. Particularly, the aluminum content of the zeolite appears to be a crucial factor of the chemical behavior inside the void space. In FAU (Si/Al = 100) no reaction occurs between $Mo(CO)_6$ and C_6H_6 under thermal activation limited by the desorption of $Mo(CO)_6$, whereas in $Na_{85}FAU$, $Mo(CO)_6$ reacts thermally as in the absence of added reagent to form anchored subcarbonyl $Mo(CO)_n$ ($n = 5, 4, 3$) species. The nature of the counterbalancing charge cations is an additional factor of the chemical behavior within the void space. Earlier papers related to arenes or $Mo(CO)_6$ sorbed alone in faujasitic zeolites and to the cosorption provide theoretical and experimental support through the siting location and dynamic behaviors of the C_6H_6 and $Mo(CO)_6$ molecules in faujasitic zeolites, thus a coherent interpretation of the chemical behavior between $Mo(CO)_6$ and C_6H_6 inside the void space of the faujasitic zeolites can be proposed.

In siliceous FAU, the $Mo(CO)_6$ and C_6H_6 molecules are not located at specific sites, they are randomly distributed in the void space. The dynamic behavior of benzene molecules sorbed alone is largely dominated by intracavity motions at room temperature. At 400 K, the benzene molecule is considerably more mobile and exhibits cage-to-cage diffusion. After cosorption in FAU, the motions of $Mo(CO)_6$ and C_6H_6 approach the rapid isotropic limit of liquids. The chemical behavior between $Mo(CO)_6$ and C_6H_6 is found to be analogous to that observed in solution.

In $Na_{56}FAU$, the benzene molecule is facially located to the SII sodium cation or in the plane of the window [16]. Dynamic studies indicate intracavity "cartwheel" and "skateboard" hopping mechanisms whereas the diffusion is determined simply by the site-to-window hopping rate. The kinetic motions are found to be slower than in the siliceous analog. Similar trends have been predicted for $Mo(CO)_6$. In the presence of $Mo(CO)_6$, the C_6H_6 molecules are predicted to be facially located to the SII cation or in the window as determined for C_6H_6 sorbed alone, whereas $Mo(CO)_6$ at low coverage is held within the supercage in close proximity of benzene molecules. The diffusion of the reagents is probably hindered at higher coverages. The enhancement of the reaction rate at relatively low coverage can be attributed to: (i) the close proximity of the reagents in the supercage, (ii) the intense electrostatic field gradient, and (iii) the concerted mechanism of the dissociation of $Mo(CO)_6$ with the coordination of framework oxygen atoms and slippage of the $Mo(CO)_3$ group to the arene molecule. The substitutional affinity of the grafted $Mo(CO)_3$ depends both on the basicity of the framework oxygen atoms and on the nature of the entering arene. The slippage probably proceeds *via* $Mo(CO)_3(\eta^{2y}\text{-}C_6H_6)(O_z)_{3-y}$ ($y = 1, 2$) intermediates without any displacement of the C_6H_6 molecule from its site [90]. Indeed, after the reaction, the

$Mo(CO)_3(\eta^6\text{-}C_6H_6)$ species is predominantly anchored *via* the facially oriented C_6H_6 ligand to the SII cation.

In Na_{85}FAU zeolites, the C_6H_6 sorbed alone is predicted to be facially coordinated to the SII or SIII cations whereas at low coverage the $Mo(CO)_6$ molecule sorbed alone is predominantly located within the supercage. In the presence of C_6H_6 no stable sorption site for $Mo(CO)_6$ is predicted in the same cavity. The high basicity of the framework oxygen atoms stabilized the subcarbonyl $Mo(CO)_3$ species through the coordination with the four-ring oxygen atoms. Even coordinated to the zeolite framework, the $Mo(CO)_3$ group remains mobile, however, the exchange from the framework oxygen atoms to the arene is not effective.

The activity of the anchored $Mo(CO)_n$ ($n=5$, 4, 3) species within the void space of faujasitic zeolites as active species to hydrogenation and isomerization of dienes may be due to their abilities to coordinate substrates at the expense of $Mo\text{–}O_z$ bonds [34,35]. From a coordination chemistry point of view, the internal surface appears to behave as a multidentate multisite anionic ligand [31]. In addition to the molecular sieves properties, the role of the support is crucial particularly through the basicity of the framework oxygen atoms and the nature of the extraframework cations. The aluminum content and the extraframework cation are means to optimize the faujasitic zeolite syntheses in view of the expected catalytic properties. However, the availability of open coordination sites does not appear as the rate-determining step of the catalytic reaction, the catalytic pathway includes the sequential complexation, functionalization and liberation of unsaturated hydrocarbons which constitute one of the most important reaction sequences in catalytic organometallic synthesis.

Acknowledgements

I thank those members of the LASIR who have directly contributed to the development of the work described in this review: Drs. Hélène Des Grousilliers, Marielle Le Maire, Gabrielle Ginestet and Jacky Laureyns. I also acknowledge those members of the LASIR who have constantly been involved in helpful and stimulating discussions, Drs. Daniel Bougeard, Christophe Depecker, Denis Dumont, Constantin Smirnov and Bernard Sombret. The Centre d'Etudes et de Recherches Lasers et Applications (CERLA) is supported by the ministère de la Recherche, Région Nord/Pas de Calais and the Fonds Européen de Développement Economique des Régions.

References

[1] D.C. Bailey, S.H. Langer, Chem. Rev. 81 (1981) 109.
[2] J.E. Maxwell, Adv. Catal. 31 (1982) 1.
[3] B.C. Gates, L. Guczi, H. Knözinger, Metal Clusters in Catalysis, Elsevier, Amsterdam, 1986.
[4] J. Goldwasser, S.M. Fang, M. Houalla, W.K. Hall, J. Catal. 115 (3) (1989) 4.

[5] R. Alves, D. Ballivet-Tkatchenko, G. Goudurier, N. Duc Chau, M. Santra, Bull. Soc. Chim. France 3 (1985) 386.
[6] M.C. Connaway, B.E. Hanson, Inorg. Chem. 25 (1986) 1445.
[7] R.L. Schneider, R.F. Howe, K.L. Watters, Inorg. Chem. 27 (1988) 4030.
[8] T. Bein, S.J. McLain, D.R. Corbin, R.D. Farlee, K. Moller, G.D. Stucky, G. Woolery, D. Sayers, J. Am. Chem. Soc. 110 (1988) 1801.
[9] G.A. Ozin, D.M. Haddelton, C.J. Gil, J. Phys. Chem. 93 (1989) 6710.
[10] C. Brémard, E. Denneulin, C. Depecker, P. Legrand, Struct. React. Surf. (1989) 219.
[11] A. Borvornwattananont, K. Moller, T. Bein, J. Phys. Chem. 93 (1989) 4205.
[12] Z. Zhang, W.M.H. Sachtler, Polyhedron 10 (1991) 673.
[13] X. Li, G.A. Ozin, S. Özkar, J. Phys. Chem. 95 (1991) 4463.
[14] M.R. Steele, P.M. Macdonald, G.A. Ozin, J. Am. Chem. Soc. 115 (1993) 7285.
[15] C. Huber, K. Moller, T. Bein, J. Phys. Chem. 98 (1994) 12067.
[16] G. Coudurier, H. Gallezot, H. Praliaud, M. Primet, B. Imelik, C.R. Acad. Sci. Paris C 282 (1976) 311.
[17] S. Abdo, R.F. Howe, J. Phys. Chem. 87 (1983) 1713.
[18] Y. You-Sing, R.F. Howe, J. Chem. Soc., Faraday Trans. I 82 (1986) 2887.
[19] S. Özkar, G.A. Ozin, K. Moller, T. Bein, J. Am. Chem. Soc. 112 (1990) 9575 and references cited therein
[20] A. Zecchina, S. Bordiga, E. Escalona Platero, C. Otero Arean, J. Catal. 125 (1990) 568.
[21] J.M. Coddington, R.F. Howe, Y.S. Yong, K. Asakura, K. Iwazawa, J. Chem. Soc., Faraday Trans. 86 (1990) 1015.
[22] G.A. Ozin, S. Özkar, P. Macdonald, J. Phys. Chem. 94 (1990) 6939.
[23] K. Moller, T. Bein, S. Özkar, G.A. Ozin, J. Phys. Chem. 95 (1991) 5276.
[24] R. Jelinek, S. Özkar, H.O. Pastore, A. Malek, G.A. Ozin, J. Am. Chem. Soc. 115 (1993) 563.
[25] O.H. Pastore, G.A. Ozin, A.J. Poë, J. Am. Chem. Soc. 115 (1993) 1215.
[26] C. Brémard, G. Ginestet, J. Laureyns, M. Le Maire, J. Am. Chem. Soc. 117 (1995) 9274.
[27] C. Brémard, G. Ginestet, M. Le Maire, J. Am. Chem. Soc. 118 (1996) 12724.
[28] G.A. Ozin, C. Gil, J. Chem. Rev. 89 (1989) 1749 and references cited therein
[29] G.A. Ozin, A. Kuperman, A. Stein, Adv. Mater. 101 (1989) 373 and references cited therein
[30] G.D. Stucky, J. Mac Dougall, Science 247 (1990) 669 and references cited therein
[31] G.A. Ozin, S. Özkar, Chem. Mater. 4 (1992) 511.
[32] G.A. Ozin, M.R. Steele, A. Holmes, J. Chem. Mater. 6 (1994) 999.
[33] K.J. Balkus, Jr., A.G. Gabrielow, in: N. Herron, D.R. Corbin (Eds.), Inclusion Chemistry with Zeolites: Nanoscale Materials by Design, Kluwer Academic Publishers, Dordrech, 1995.
[34] Y. Okamoto, H. Kane, T. Imanaka, Catal. Lett. 2 (1989) 335.
[35] Y. Okamoto, H. Onimatsu, M. Hori, I. Inui, T. Imanaka, Catal. Lett. 12 (1992) 239.
[36] H. Koller, A.R. Overweg, R.A. van Santen, J.W. de Haan, J. Phys. Chem. 101 (1997) 1754 and references cited therein
[37] G.A. Ozin, S. Özkar, R.A. Prokopowicz, Acc. Chem. Res. 25 (1992) 553.
[38] W.M. Meier, D.H. Olson, S.C. Baerlocher, Atlas of Zeolite Structure Types, Int. Zeolite Assoc., Butterworth–Heinemann, London, 1996.
[39] E.M. Flanigen, J.C. Jansen, S.T. Wison, in: H. van Bekkum, E.M. Flanigen, J.C. Jansen (Eds.), Introduction to Zeolite Science and Practice, Elsevier, Amsterdam, 1991.
[40] C. Brémard, M. Le Maire, J. Mol. Struct. 349 (1995) 49.
[41] J.A. Hriljac, M.M. Eddy, A.K. Cheetham, J.A. Donohue, G.J. Ray, J. Solid State Chem. 106 (1993) 66.
[42] A.N. Fitch, H. Jobic, A. Renouprez, J. Phys. Chem. 90 (1986) 1311.
[43] J.L. Lievens, W.J. Mortier, K.J. Chao, J. Phys. Chem. Solids 53 (1992) 1163.
[44] D.H. Olson, Zeolites 15 (1995) 441.
[45] C. Forano, R.C.T. Slade, E. Krogh Andersen, I.G. Krogh Andersen, E. Prince, J. Solid State Chem. 82 (1989) 95.
[46] G.R. Eulenberger, D.P. Shoemaker, J.G. Feil, J. Phys. Chem. 71 (1967) 1812.
[47] H. Koller, B. Burger, A.M. Schneider, G. Engelhardt, J. Weitkamp, Microporous Mater. 5 (1995) 219.

[48] M. Czjzek, H. Jobic, A.N. Fitch, T. Vogt, J. Phys. Chem. 96 (1992) 1535.
[49] W. Loewenstein, Am. Mineral 39 (1942) 92.
[50] T. Takaishi, M. Kato, K. Itabashi, J. Phys. Chem. 98 (1994) 5742.
[51] N.Y. Chen, T.F. Degnan, Jr., C. Morris Smith, in: Molecular Transport and Reaction in Zeolites, VCH, New York, Cambridge, Weinheim, 1994.
[52] G. Schrimpf, M. Schlenkrich, J. Brickmann, P. Bopp, J. Phys. Chem. 196 (1992) 7404.
[53] W.J. Mortier, Compilation of extra-framework sites in zeolites, issued by the Commission of the International Zeolite Association, 1981.
[54] Y.S. Yon, R.F. Howe, A.E. Hughes, H. Jaeger, B.A. Sexton, J. Phys. Chem. 91 (1987) 6331.
[55] P.A. Cybulski, D.J. Gillis, M.C. Baird, Inorg. Chem. 32 (1993) 460.
[56] C.L. Tway, T.M. Apple, Inorg. Chem. 31 (1992) 2885.
[57] C. Brémard, H. Des Grousilliers, Raman Spectrosc. 22 (1991) 125.
[58] C. Brémard, D. Bougeard, Adv. Mater. 7 (1995) 10.
[59] C. Brémard, C. Depecker, H. Des Grousilliers, P. Legrand, Appl. Spectrosc. 45 (1991) 1278.
[60] P. Kubelka, F. Munck, Z. Tech. Physik 12 (1931) 593.
[61] L. Uytterhoeven, D. Dompas, W.J. Mortier, J. Chem. Soc., Faraday Trans. 3 (1992) 633.
[62] S.P. Arnesen, H.M. Seip, Acta Chim. Scand. 20 (1966) 2711.
[63] A. Jost, B. Rees, Acta Crystallogr. B 31 (1975) 2647.
[64] A. Whitaker, J.W. Jeffery, Acta Crytallogr. 23 (1967) 977.
[65] B. Rees, P. Coppens, Acta Cryst. B 29 (1973) 2515.
[66] K.L. Kunze, E.R. Davidson, J. Phys. Chem. 96 (1992) 2129.
[67] C.W. Bauschlicher Jr.,, P.S. Bagus, J. Phys. Chem. 81 (1984) 5889.
[68] B. Folkeson, R. Larsson, J. Electron Spectrosc. Relat. Phenom. 81 (1990) 5889.
[69] J. Li, G. Schreckkenbach, T. Ziegler, J. Phys. Chem. 98 (1994) 4838 and publications cited therein
[70] S.M. Auerbach, N.J. Henson, A.K. Cheetham, H.I. Metiu, J. Phys. Chem. 99 (1995) 10600.
[71] A. De Mallmann, D. Barthomeuf, Zeolites 8 (1988) 292.
[72] A. De Mallmann, D. Barthomeuf, J. Phys. Chem. 93 (1989) 5636.
[73] K. Krause, E. Geidel, J. Kindler, H. Förster, H. Böhlig, J. Chem. Soc., Chem. Commun. (1995) 2481.
[74] K. Krause, E. Geidel, J. Kindler, FörsterH., K.S. Smirnov, Vibrational Spectrosc. 12 (1996) 45.
[75] D. Dumont, thesis, University Lille, France, 1996.
[76] Y. Okamoto, A. Maezawa, H. Kane, T. Imanaka, J. Chem. Soc., Faraday Trans. I 84 (1989) 851.
[77] Y. Okamoto, T. Imanaka, K. Asakura, Y. Iwasawa, J. Phys. Chem. 95 (1991) 3700 and references cited therein
[78] Y. Okamoto, Y. Inui, H. Onimatsu, T. Imanaka, J. Phys. Chem. 95 (1991) 4596.
[79] W.M. Shirley, N. Abdul-Manan, J.S. Frye, Inorg. Chem. 27 (1988) 3846.
[80] W.M. Shirley, C.A. Powers, C.L. Tway, Colloids and Surfaces 45 (1990) 57.
[81] H. Klein, H. Fuess, G. Schrimpf, J. Phys. Chem. 100 (1996) 11101.
[82] L.M. Bull, N.J. Henson, A.K. Cheetham, J.M. Newsam, S.J. Heyes, J. Phys. Chem. 97 (1993) 11776.
[83] C. Kirschhock, H. Fuess, Microporous Mater. 2 (1994) 261.
[84] M. Czjzek, H. Jobic, M. Bee, J. Chem. Soc., Faraday Trans. I 87 (1991) 3455.
[85] H. Jobic, A. Renouprez, A.N. Fitch, Lauter, J. Chem. Soc., Faraday Trans. I 83 (1987) 3199.
[86] H. Boulet-Des Grousilliers, thesis, University Lille, France, 1991.
[87] M. Eic, M. Goddard, D.M. Ruthven, Zeolites 8 (1988) 327.
[88] R. Goyal, A.N. Fitch, H. Jobic, J. Chem. Soc., Chem. Soc. I (1990) 1152.
[89] S. Aime, D. Braga, R. Gobetto, F. Grepioni, A. Orlandi, Inorg. Chem. 30 (1991) 951.
[90] J.A.S. Howell, N.F. Ashford, D.T. Dixon, J.C. Kola, T.A. Albright, S.K. Kang, Organometallics 10 (1991) 1852.